Title
A Mathematical Model of Diffusion as a Length Sensor in Intraflagellar Transport

Author
Hendel, Nathan Lawrence

Publication Date
2020

Peer reviewed|Thesis/dissertation

A Mathematical Model of Diffusion as a Length Sensor in Intraflagellar Transport

by
Nathan Lawrence Hendel

DISSERTATION
Submitted in partial satisfaction of the requirements for degree of
DOCTOR OF PHILOSOPHY

in

Biological and Medical Informatics

in the

GRADUATE DIVISION
of the
UNIVERSITY OF CALIFORNIA, SAN FRANCISCO

Approved:

DocuSigned by:
Wallace Marshall
43941FCFA7C0447...

Wallace Marshall
Chair

DocuSigned by:
Sophie Dumont
DocuSigned by:
Bo Huang
1E7C3BA93EB54F3...

Sophie Dumont

Bo Huang

Committee Members

Dedicated to my Grandpa Ed Eberhardt,

who shared with me his delight for science and invention.

I would like to thank Prof. Wallace Marshall for his support, brilliance, and contagious enthusiasm. I would like to thank my lab-mates Athena Lin, Greyson Lewis, Amy Chang, David Bauer, Rebecca McGillivary, Jacob Kimmel, Karina Perlaza, Erik Navarro, Ulises Diaz, Connie Yan, Hiro Ishikawa, Mary Mirvis, Ben Larson, Vincent Boudreau, Sarah Reiff, Guillermina Ramirez-San Juan, Pranidhi Sood, and Tatyana Makushok for creating a supportive lab culture that values imagination and curiosity. I would like to thank Rui Ma and Hongmin Qin for being brilliant and team-oriented collaborators. I would also like to thank my thesis committee: Prof. Sophie Dumont and Prof. Bo Huang, for their guidance and expertise. I would like to thank my friends at UCSF: Paul Thomas, Pooja Suresh, Justin Biel, Sandra Catania, Daniel Asarnow, Cole Helsell, Sergei Pourmal, Sasha Dickinson, Matvei Khoroshkin, Elizabeth McCarthy, Jianhua Zhao, and Madeline Keenen for filling my days with laughter and wisdom. Lastly, I would like to thank my family: my parents Ann and Ron, my brother Ed, Uncle Doug and Aunt Lisa, and my cousins Robby and Amanda, for their unlimited support.

Contributions

This dissertation begins with a new introduction followed by the entirety of two publications. The publications are:

Hendel, Nathan L., Matthew Thomson, and Wallace F. Marshall. "Diffusion as a Ruler: Modeling Kinesin Diffusion as a Length Sensor for Intraflagellar Transport." *Biophysical Journal* 114, no. 3 (06 2018): 663–74. https://doi.org/10.1016/j.bpj.2017.11.3784.

Ma, Rui, Nathan L. Hendel, Wallace F. Marshall, and Hongmin Qin. "Speed and Diffusion of Kinesin-2 Are Competing Limiting Factors in Flagellar Length-Control Model." *Biophysical Journal* 118, no. 11 (June 2, 2020): 2790–2800. https://doi.org/10.1016/j.bpj.2020.03.034.

A Mathematical Model of Diffusion as a Length Sensor in Intraflagellar Transport

Nathan L. Hendel

Abstract

An important question in cell biology is whether cells are able to measure size, either whole cell size or organelle size. Perhaps cells have an internal chemical representation of size that can be used to precisely regulate growth, or perhaps size emerges due to constraint of nutrients. The eukaryotic flagellum is an ideal model for studying size sensing and control because its linear geometry makes it essentially one-dimensional, greatly simplifying mathematical modeling. The assembly of flagella is regulated by intraflagellar transport (IFT), in which kinesin motors carry cargo adaptors for flagellar proteins along the flagellum and then deposit them at the tip, lengthening the flagellum. The rate at which IFT motors are recruited to begin transport into the flagellum is anticorrelated with the flagellar length, implying communication between the base and the tip and possibly indicating that cells contain some mechanism for measuring flagellar length. Although it is possible to imagine many complex scenarios in which additional signaling molecules sense length and carry feedback signals to the cell body to control IFT, might the already-known components of the IFT system be sufficient to allow length dependence of IFT? Here we investigate a model in which the anterograde kinesin motors unbind after cargo delivery, diffuse back to the base, and are subsequently reused to power entry of new IFT trains into the flagellum. By mathematically modeling and simulating such a system, we are able to show that the diffusion time of the motors can in principle be sufficient to serve as a proxy for length measurement. An analytical formulation of the model predicts the effect that physical parameters have on length, motivating experiments that can validate or disprove the model.

Table of Contents

List of Figures

List of Tables

Introduction

In order to live, function, and reproduce, cells have to build a complex world within themselves that is robust and adaptive. Cells build their organelles to be the right size and shape, and they do so through self-assembly. There is no blueprint to organelles, no predetermined plan. Instead, proteins must come together in the thousands and form intracellular structures with precise shapes. This is the key question of the field of cell geometry: how do cells build themselves and their organelles to be the right sizes and shapes?

Nowhere is the importance of cell geometry as evident as in single-celled organisms. These organisms, as their name implies, consist of just one cell. They have no brain to rely on to pass down signals, and they have no tissues with neighboring cells they can rely on for support. Single-celled organisms have to build themselves to be able to swim, hunt, survive, and reproduce.

The single-celled green algae *Chlamydomonas reinhardtii* is an unassuming oval-shaped cell with two flagella that protrude out into the pond water in which it lives. Flagella (also known as cilia in eukaryotes like *Chlamydomonas*) are long whip-like appendages that protrude from the cell body. *Chlamydomonas* uses these two flagella to swim by beating them in a cyclic pattern resembling a breast stroke. The cell body is about 10 micrometers long, and each cilium is an additional 10 micrometers. *Chlamydomonas* must build its two flagella to exactly the same length in order to swim straight. The curious thing about *Chlamydomonas's* flagella is that when one is severed, it will grow back to the same length it was before it was cut (1). In fact, not only does its cut flagellum regenerate to its original length, the other flagellum will shrink as the cut one grows. It will shrink until they are the same length, and then both flagella grow back to their original length together (1). This is most likely to minimize the amount of time the cilia are

different lengths, thereby maximizing the amount of time the cell can swim straight. This demonstrates that *Chlamydomonas* has a high degree of internal geometry coordination.

Since severed flagella grow back to their original length, *Chlamydomonas* somehow knows how long its flagella should be. But *Chlamydomonas* is just one cell and does not have a brain, so perhaps "knowing" is perhaps a misleading term. Still, somehow *Chlamydomonas* has the information about its ideal flagellar length encoded within it. Could it be a length sensor that signals to the cell body how long to build its flagella? Or a scarcity of resources where a cell of a certain size cannot build past a certain length?

The question of how *Chlamydomonas* builds its flagella back to the same size every time is my research topic, and there are two reasons that make it a fruitful topic. The first is that the flagellum's linear geometry makes it an ideal system for mathematical modeling. It offers a simple system for studying how cells construct and maintain their organelles. The second is that the flagellum is a well-conserved organelle across different species, meaning its structure and protein composition is consistent in many species (2). Flagella are common organelles in cells, and are not just used for locomotion but also for sensing and generating flow (3, 4). For example, human respiratory cells use cilia to clear mucus (5). There are many human diseases caused by malfunctioning cilia, known collectively as ciliopathies, that involve a variety of symptoms affecting development by altering developmental signaling pathways as well as physiological function such as mucus clearance (6, 7). Understanding how cells regulate ciliary length could provide insight into how to cure these diseases.

In order to investigate how *Chlamydomonas* regulates the length of its flagella, it is necessary to learn the structure of the flagellum. Flagella are relatively simple organelles because they have a linear shape, and when they grow they get longer, not wider. This property simplifies

the study of their growth from a three-dimensional to a one-dimensional problem. The building process of a flagellum is fairly well understood. The internal structure of the flagellum is built out of the protein tubulin, which serves as a building block. Tubulin proteins form linear structures called microtubules, and the flagellum consists of several bundles of microtubules. The collection of microtubule bundles is sheathed by the cell membrane, analogous to a cat's tailbone surrounded by skin.

The motor protein kinesin-2 is the protein responsible for transporting tubulin from the base to the tip in a process called intraflagellar transport, or IFT (8–11). Kinesin-2 has two microtubule binding domains and uses them to walk along microtubules. Kinesins come together with other kinesins to form trains, and these trains bind a collection of proteins called IFT particles, which contain tubulin (12, 13). The train walks from the base of the cell to the tip, at which point it deposits the tubulin. The tubulin binds to the end of one of the microtubules, elongating the microtubule and thus the flagellum. This process resembles a group of people carrying a sack of bricks down a hallway. Unlike humans however, kinesins can only walk in one direction. The microtubule has a directionality due to the asymmetric structure of the tubulin subunits. One end is called the plus end because tubulin addition is faster at that end. Kinesin can only walk toward the plus end at the tip because of its own asymmetry.

While the tubulin has been incorporated onto the end of the microtubule, the IFT particle (the sack in the metaphor) must return to the base. This is where dynein comes in. Dynein is a motor protein conceptually similar to kinesin because it can walk along microtubules carrying cargo, except it walks in the other direction. Dyneins carry the IFT particle from the tip back to the base to be reused in IFT (8, 9).

Intraflagellar transport is required not just for building flagella in the first place, but also for maintaining existing flagella (14). The IFT particles that are brought back by dynein then pick up tubulin and bind to another train of kinesin for transport to the tip. But even though IFT happens throughout the lifetime of the cell, the flagellum does not get longer forever. Tubulin at the tip can unbind from the microtubule, shortening the flagellum. This decay happens throughout the lifetime of the cell as well, and we believe that the rate of decay is constant and independent of the flagellar length (15). The flagellum grows through IFT and shrinks through decay, so the overall growth rate is the difference between the rate of IFT and the rate of decay. When the rate of IFT bringing tubulin to the tip is greater than the rate of decay, the flagellum will grow. When the rate of IFT is smaller than the rate of decay, the flagellum will shrink. The reason *Chlamydomonas's* flagella have constant lengths for most of their lives is that these two length factors reach equilibrium: the rate of IFT exactly equals the rate of decay. This equilibrium is a "steady state," and this type of model is referred to as the "balance point" model.

A regenerating flagellum grows very quickly when the length is small. This is because the flagellum is shorter, so it takes less time for IFT to reach the tip and less time for the dyneins to bring the IFT particles back. The growth rate decreases as the flagellum grows, and the flagellum gradually approaches its steady-state length. Since flagellar decay is length-independent, and the growth rate is length-dependent, the rate of IFT (which is the difference between these two) must be length-dependent (15, 16). This means that the cell modulates the rate of IFT based on the length of the flagellum.

Evidence of this came in an experiment imaging IFT injection. Injection is the IFT initiation process, in which kinesins leave the cell body and enter the flagellum. The compartment of the cell connecting the cell body to the flagellum is called the transition zone,

representing the distal end of the basal body which nucleates the flagellum. In the basal body, kinesins come together to form trains, pick up their IFT particles, and collect tubulin (17). The trains are then launched through the transition zone into the flagellum to begin their transport. IFT trains walk at a constant speed along the flagellum, so the rate of injection is essentially the same as the rate of IFT, which is the same as the rate of flagellar growth. The study that validated the balance point model showed a very curious finding: the rate of injection is anticorrelated with the length of the flagellum (18). The longer the flagellum is, the less often IFT trains are injected. The observation made was that the distribution of IFT trains injected into the flagellum resembles an avalanche. Avalanches come from the piling up of some material like sand or rocks, and the pile is stable until it reaches a critical threshold of amount of material. Once it reaches this threshold, some of the material will fall down and exit the pile. The observation made in *Chlamydomonas* flagella is that the distribution of sizes of IFT trains and the distribution of dwell times between injection events follow the same stochastic pattern as avalanching. While the inner workings of the transition zone are not well understood, this pattern could happen if the kinesins were squeezing through a pore (19). So while we do not know the physical mechanism of avalanching, experiments have shown that accumulation of kinesin motors in the basal body leads to injection events. The longer the flagellum is, the less often the basal body reaches the critical threshold of kinesin accumulation.

This confirms the balance point model's claim that IFT is length-dependent, but it raises a fundamental question: how does the basal body know how long the flagellum is? The basal body and the tip of the flagellum are separated by the length of the flagellum, yet somehow the basal body can sense how long the flagellum is and how much IFT material to inject. At steady state, the length of the flagellum is roughly the same as the length of the cell body, so

Chlamydomonas has a tough engineering challenge. This single cell has to have a method for sensing long lengths.

Conceptually this is analogous to the action at a distance problem that plagues physicists when they try to explain how two distant objects can interact. How does a positive charge "know" to move towards a negative charge? How does the Earth "know" to revolve around the Sun even though they are far away? These problems are solved with particles that are transmitted from one body to the other. Biology is often more complicated, so the puzzle here is to figure out how the tip of the flagellum transmits information about its length down to the cell body.

Several models have been theorized. The goal now is to develop each model using theory so that we can motivate experiments that will reject or validate the model. One recent theory is that the IFT particles can measure the time it takes them to go from the base of the cell to the tip and back, and the cell is tuned to build its flagella to a length that would register as a certain amount of time for the IFT particles (20). This theory, called the "time-of-flight model" was developed and tested by Ishikawa and Marshall, who used theory to determine that slowing down dynein's transport from the tip to the base (called "retrograde transport") should decrease injection (21). When they used a *Chlamydomonas* mutant with lower retrograde transport speeds, they found the opposite: injection increased. Thus, they ruled out the time-of-flight model.

Another model considers the ion channels which are regularly spaced within the flagellum, transporting charged ions to the cell body. The "ciliary current" model claims these ion channels generate a current that acts as a length signal (22–24). The flagellum adds more ion channels as it grows, so the longer it is, the more ions it has within it. These charged ions travel down to the cell body and generate a current. In this model, the cell body recognizes the amount of charge, and the cell is tuned to build its flagella to a length that would register as a certain

amount of current from the flagella. This model is still considered possible, as experimental data has not ruled it out.

The other model that has not yet been ruled out is the diffusion model, which is the focus of this dissertation. In the diffusion model, the flagellar length is determined by a gradient of concentration of a diffusive molecule. In this system, we hypothesize that the diffusive molecule is the kinsin-2 motors that transport the IFT cargo to the tip. The concept here is that the kinesin-2 motors are injected, walk to the tip, deposit the tubulin (elongating the flagellum), and then unbind. Once they are unbound, they begin diffusing.

Diffusion is the process in which small objects move randomly through small thermal fluctuations in the material the objects are immersed in. If a large number of small objects are undergoing diffusion, the cumulative effect of the random motion is that the objects spread out. For example, if you have a tube that is closed on one end, and you put a drop of food coloring inside the tube at the closed end, the food coloring will spread out and eventually exit out the open end.

In the diffusion model of flagellar length control, the kinesins start diffusing once they reach the tip. Since the flagellum is wrapped in a membrane and the only escape is back at the base, the diffusing kinesins will always eventually make it back, just like the food coloring in the tube. Once they make it back, they accumulate in the basal body. Once enough of them have accumulated in the basal body, an avalanche of kinesins is injected into the flagellum to be re-used in IFT. This solves the issue of the cell injecting kinesin less often when the flagellum is longer: if the flagellum is longer, it takes longer for kinesins to reach the base, so it takes longer for enough kinesins to accumulate to trigger an avalanching event. When the flagellum gets longer and the rate of injection is small enough that it exactly balances out the decay rate, steady

state has been achieved. If the flagellum is too short, the growth rate will be higher than the decay rate. If it is too long, the decay rate wins out. This is a stable equilibrium, and will result in the same steady-state length every time the flagellum grows.

A critical piece of experimental evidence was published at the time as I was developing the model. Alex Chien and Ahmet Yildiz made an innovation in microscopy that allowed them to track a single train of kinesin-2 motors during their entire journey inside the flagellum, and found that the kinesin-2 motors indeed diffuse inside the flagellum once they reach the tip (25). They also showed that the dyneins that carry the IFT particles back to the base are themselves brought to the base as passengers on the kinesin IFT trains, but the kinesins are not brought back by the dyneins. Since we know that the kinesins are diffusing, the modeling question narrows to: is the diffusive return of kinesin sufficient to achieve length control?

This dissertation brings together the two publications that I wrote with my collaborators and published during the course of my doctoral studies. The first, "Diffusion as a Ruler: Modeling Kinesin Diffusion as a Length Sensor for Intraflagellar Transport," uses mathematics and simulations to show that kinesin diffusion is indeed sufficient to achieve length control (26). We also showed that if both flagella are drawing from a common pool of tubulin, the shrinking effect of the intact flagella occurs when the other flagella is cut, matching experimental observation. This paper was written primarily with my advisor Prof. Wallace Marshall, and we incorporated critical input from Prof. Matt Thomson, a UCSF faculty member at the time. This discovery means we can generate hypotheses that will test the theory. Some of this is done in this first paper, but it is much more developed in the second paper, "Speed and Diffusion of Kinesin-2 Are Competing Limiting Factors in Flagellar Length-Control Model" 12/16/20 11:54:00 AM. This second paper was a result of a team of Prof. Marshall, Dr. Rui Ma, Prof. Hongmin Qin, and

me. This paper explores the predicted flagellar lengths based on the physical parameters of the system using the diffusion model as the theory. This lets us generate hypotheses to test in the lab. For example, we can use the results of this study to predict how much length would change if we tested a mutant with IFT trains that move half as fast. The advantage of this form of analysis is that we can motivate experiments that we never would have thought to do in order to test the theory. In the discussion section of the paper, we discuss the possibility that a completely overlooked parameter in the length control field, the beating of the flagella as the cell swims, could have an effect on length.

The diffusion model is the simplest solution to the puzzle of length control given the experimental evidence collected over the years. It is an elegant model, because it circumvents the need for the cell to have a black-box signaling mechanism with a currently unknown signaling source, and instead asserts that the cell can harness the passive physics of diffusion to build itself. Now that the diffusion model is well-developed, it is ripe for experimentalists to go to the lab and perform experiments to test the theory.

References

1. Rosenbaum, J.L., J.E. Moulder, and D.L. Ringo. 1969. Flagellar elongation and shortening in Chlamydomonas. The use of cycloheximide and colchicine to study the synthesis and assembly of flagellar proteins. *J. Cell Biol.* 41:600–619.

2. Mitchell, D.R. 2004. Speculations on the evolution of 9+2 organelles and the role of central pair microtubules. *Biol. Cell*. 96:691–696.

3. Praetorius, H.A., and K.R. Spring. 2003. The renal cell primary cilium functions as a flow sensor. *Curr. Opin. Nephrol. Hypertens.* 12:517–520.

4. Guirao, B., and J.-F. Joanny. 2007. Spontaneous creation of macroscopic flow and metachronal waves in an array of cilia. *Biophys. J.* 92:1900–1917.

5. Sleigh, M.A. 1990. Ciliary adaptations for the propulsion of mucus. *Biorheology*. 27:527–532.

6. Badano, J.L., N. Mitsuma, P.L. Beales, and N. Katsanis. 2006. The ciliopathies: an emerging class of human genetic disorders. *Annu. Rev. Genomics Hum. Genet.* 7:125–148.

7. Zariwala, M.A., M.R. Knowles, and H. Omran. 2007. Genetic defects in ciliary structure and function. *Annu. Rev. Physiol.* 69:423–450.

8. Cole, D.G., D.R. Diener, A.L. Himelblau, P.L. Beech, J.C. Fuster, and J.L. Rosenbaum. 1998. Chlamydomonas kinesin-II-dependent intraflagellar transport (IFT): IFT particles contain proteins required for ciliary assembly in Caenorhabditis elegans sensory neurons. *J. Cell Biol.* 141:993–1008.

9. Scholey, J.M. 2003. Intraflagellar transport. *Annu. Rev. Cell Dev. Biol.* 19:423–443.

10. Taschner, M., and E. Lorentzen. 2016. The Intraflagellar Transport Machinery. *Cold Spring Harb. Perspect. Biol.* 8.

11. Lechtreck, K.F., J.C. Van De Weghe, J.A. Harris, and P. Liu. 2017. Protein transport in growing and steady-state cilia. *Traffic Cph. Den.* 18:277–286.

12. Stepanek, L., and G. Pigino. 2016. Microtubule doublets are double-track railways for intraflagellar transport trains. *Science*. 352:721–724.

13. Vannuccini, E., E. Paccagnini, F. Cantele, M. Gentile, D. Dini, F. Fino, D. Diener, C. Mencarelli, and P. Lupetti. 2016. Two classes of short intraflagellar transport train with different 3D structures are present in Chlamydomonas flagella. *J. Cell Sci.* 129:2064–2074.

14. Kozminski, K.G., P.L. Beech, and J.L. Rosenbaum. 1995. The Chlamydomonas kinesin-like protein FLA10 is involved in motility associated with the flagellar membrane. *J. Cell Biol.* 131:1517–1527.

15. Marshall, W.F., and J.L. Rosenbaum. 2001. Intraflagellar transport balances continuous turnover of outer doublet microtubules. *J. Cell Biol.* 155:405–414.

16. Marshall, W.F., H. Qin, M.R. Brenni, and J.L. Rosenbaum. 2005. Flagellar Length Control System: Testing a Simple Model Based on Intraflagellar Transport and Turnover. *Mol. Biol. Cell*. 16:270–278.

17. Deane, J.A., D.G. Cole, E.S. Seeley, D.R. Diener, and J.L. Rosenbaum. 2001. Localization of intraflagellar transport protein IFT52 identifies basal body transitional fibers as the docking site for IFT particles. *Curr. Biol. CB*. 11:1586–1590.

18. Ludington, W.B., K.A. Wemmer, K.F. Lechtreck, G.B. Witman, and W.F. Marshall. 2013. Avalanche-like behavior in ciliary import. *Proc. Natl. Acad. Sci.* 110:3925–3930.

19. Dishinger, J.F., H.L. Kee, P.M. Jenkins, S. Fan, T.W. Hurd, J.W. Hammond, Y.N.-T. Truong, B. Margolis, J.R. Martens, and K.J. Verhey. 2010. Ciliary entry of the kinesin-2 motor KIF17 is regulated by importin-β2 and Ran-GTP. *Nat. Cell Biol.* 12:703–710.

20. Sloboda, R.D., and J.L. Rosenbaum. 2007. Making sense of cilia and flagella. *J. Cell Biol.* 179:575–582.

21. Ishikawa, H., and W.F. Marshall. 2017. Testing the time-of-flight model for flagellar length sensing. *Mol. Biol. Cell*. 28:3447–3456.

22. Pazour, G.J., B.L. Dickert, Y. Vucica, E.S. Seeley, J.L. Rosenbaum, G.B. Witman, and D.G. Cole. 2000. Chlamydomonas IFT88 and Its Mouse Homologue, Polycystic Kidney Disease Gene Tg737, Are Required for Assembly of Cilia and Flagella. *J. Cell Biol.* 151:709–718.

23. Rosenbaum, J. 2003. Organelle size regulation: length matters. *Curr. Biol. CB*. 13:R506-507.

24. Johnson, K.A., and J.L. Rosenbaum. 1993. Flagellar regeneration in Chlamydomonas: a model system for studying organelle assembly. *Trends Cell Biol.* 3:156–161.

25. Chien, A., S.M. Shih, R. Bower, D. Tritschler, M.E. Porter, and A. Yildiz. 2017. Dynamics of the IFT machinery at the ciliary tip. *eLife*. 6:e28606.

26. Hendel, N.L., M. Thomson, and W.F. Marshall. 2018. Diffusion as a Ruler: Modeling Kinesin Diffusion as a Length Sensor for Intraflagellar Transport. *Biophys. J.* 114:663–674.

Chapter 1

Diffusion as a Ruler: Modeling Kinesin Diffusion as a Length Sensor for Intraflagellar Transport

The text of this chapter of the dissertation is a reprint of the material as it appears in Biophysical Journal. The co-authors listed in this publication directed and supervised the research that form the basis for this chapter of the dissertation. Below is a copy of the entirety of the publication:

Hendel, Nathan L., Matthew Thomson, and Wallace F. Marshall. "Diffusion as a Ruler: Modeling Kinesin Diffusion as a Length Sensor for Intraflagellar Transport." *Biophysical Journal* 114, no. 3 (February 6, 2018): 663–74. https://doi.org/10.1016/j.bpj.2017.11.3784.

Abstract

An important question in cell biology is whether cells are able to measure size, either whole cell size or organelle size. Perhaps cells have an internal chemical representation of size that can be used to precisely regulate growth, or perhaps size is just an accident that emerges due to constraint of nutrients. The eukaryotic flagellum is an ideal model for studying size sensing and control because its linear geometry makes it essentially one-dimensional, greatly simplifying mathematical modeling. The assembly of flagella is regulated by intraflagellar transport (IFT), in which kinesin motors carry cargo adaptors for flagellar proteins along the flagellum and then deposit them at the tip, lengthening the flagellum. The rate at which IFT motors are recruited to begin transport into the flagellum is anticorrelated with the flagellar length, implying some kind of communication between the base and the tip and possibly indicating that cells contain some mechanism for measuring flagellar length. Although it is possible to imagine many complex scenarios in which additional signaling molecules sense length and carry feedback signals to the cell body to control IFT, might the already-known components of the IFT system be sufficient to allow length dependence of IFT? Here, we investigate a model in which the anterograde kinesin motors unbind after cargo delivery, diffuse back to the base, and are subsequently reused to power entry of new IFT trains into the flagellum. By mathematically modeling and simulating such a system, we are able to show that the diffusion time of the motors can in principle be sufficient to serve as a proxy for length measurement. We found that the diffusion model can not only achieve a stable steady-state length without the addition of any other signaling molecules or pathways, but also is able to produce the anticorrelation between length and IFT recruitment rate that has been observed in quantitative imaging studies.

1. Introduction

How does the cell control the size of its organelles? This question has been puzzling cell biologists for decades. Cells must have a robust and efficient procedure for building organelles with a specific size and shape. The stochastic kinetics of polymerization typically leads to formation of structures with widely varying sizes in the absence of any size-dependent assembly or disassembly processes (1). But organelles are thousands of times bigger than the materials used to build them. How can molecular pathways of assembly sense and respond to organelle size to yield organelles of a necessary size for proper function? This problem is extremely difficult to solve in the general case considering the many different types of organelles and their often highly complex structures. In order to simplify the problem, we will just consider the eukaryotic flagellum. Flagella (also known as cilia) are long whip-like appendages protruding from certain cells and are used for both locomotion and sensing. Unlike a prokaryotic flagellum, which is made of a tube of a single polymer, the eukaryotic flagellum is a more complex structure made of nine microtubule doublets underlying a protrusion of the plasma membrane. These doublets are nucleated by the basal body. The flagellum is the perfect organelle to model mathematically because it has a linear geometry: when it grows, it gets longer but not wider, making it essentially a one-dimensional organelle.

Here, we will consider the flagella of *Chlamydomonas reinhardtii,* a eukaryotic alga that has two flagella. When *Chlamydomonas* develop, their flagella grow with decelerating kinetics, ultimately leveling out to a steady-state length (2). This slow-down in growth suggests that some part of the flagellum-building mechanism is feedback-regulated by length such that growth ceases when the flagellum reaches a certain length. In cells with two flagella, an interaction is observed such that when one flagellum is severed, the other flagellum will shorten until the two flagella reach the same length (2). This length equalization also suggests some form of feedback

control between the two flagella. The present study examines how these types of length-dependent control of assembly might happen.

Most of the flagellum-building machinery is known. To build a flagellum, cells use a process called intraflagellar transport, or IFT (3, 4, 5, 6). IFT, diagrammed in Figure 1.1A, is mediated by complexes of approximately 20 polypeptides called IFT proteins, which contain numerous protein-protein interaction domains capable of binding the building blocks of flagella such as tubulin and axonemal dynein arms. These IFT protein complexes associate into linear arrays known as "trains" (7,8). IFT trains are pulled to the distal tip by heterotrimeric kinesin-2 motors (9,10). Upon reaching the tip, the contents of the cargo add to the length of the flagellum. Flagella are thus undergoing continuous incorporation of new tubulin and other building blocks. To counter this, tubulin is continually removed from the flagellar tip at a constant, length-independent rate (11). Since this decay rate is constant, in order to achieve a steady state, the rate of IFT must be length-dependent (11,12).

IFT trains are recruited from docking sites on the basal bodies (13) into the flagellum to begin transport through a process called injection. The physical mechanism of injection is unknown, but it is thought to involve IFT trains moving through some sort of selective pore or barrier similar to a nuclear pore (14, 15). While the molecular details of the injection process remain unclear, quantitative imaging studies (16) have revealed that motors are recruited into the flagellum according to a pattern of dynamics similar to how sand dropped onto a sandpile will fall off (avalanche) if the pile is high enough. For example, the more time elapses before a train is injected, the larger the train is, and the larger a train is injected, the more time will elapse before the next injection event. The sizes of the injection events are power-law distributed, similar to the size of avalanching events in sandpiles and other avalanching systems. These

similarities suggest a simple model in which IFT proteins and motors accumulate at the basal body, gradually exerting more force on the pore until eventually a cluster of motors pushes through the pore, injecting a train (16). In such a scenario the rate at which motors accumulate at the base would ultimately be what determines the rate of injection.

Quantitative live cell imaging (16, 17) has shown that the rate of injection of motors is anticorrelated with the length of the flagellum. Furthermore, quantitative analysis of IFT cargo loading suggests that cargo loading is also length-dependent (18). These length-dependencies imply some kind of communication between the base and the tip. Perhaps some sort of additional signaling pathways have evolved that can sense length, transduce length into some form of molecular signal, and then use this signal to modulate the injection of IFT proteins at the base of the flagellum. Several possible models for length-sensing pathways have been described and analyzed (16, 19). Each of these models invokes additional molecular pathways that could transduce length into a signal that would gate entry of IFT particles through a pore. But what if no such additional pathway exists? Might the IFT machinery itself be capable of responding to changes in flagellar length?

Here we consider a model that takes into account the return of IFT motors from the flagella tip. IFT is a cyclical process: IFT trains and motors move to the tip, deliver cargo, return to the cell body, and then are re-injected (20). Experimental data has addressed how motors are recruited into the flagellum, how motors get to the tip, and how the flagellum grows and shrinks. Two aspects of the IFT system that have been less intensively studied are how motors are sent to the pool at the basal body and what happens to the anterograde kinesin motors after they deliver their cargo to the tip. We propose a simple model to answer both of these questions: after dropping off their cargo, the kinesin motors unbind and diffuse back to the base, where they are

then added back into the pool of accumulated motors waiting to be injected. The initial evidence for a diffusive return of the kinesin motor was the failure to observe processive retrograde traces in kymographs of IFT using GFP-tagged kinesin subunits (17), and the fact that when retrograde IFT is inhibited, IFT proteins accumulate at the flagellar tip, but the kinesin motor does not (21). Direct tracking of individual trains by a novel bleach-gate method has shown that kinesin undergoes diffusion after dissociation from trains at the distal tip (22). In considering simple models for IFT that incorporate diffusive return of kinesin, we observed that the rate of diffusive return of kinesin motors to the pool at the flagellar base can serve as a proxy for flagellar length measurement, leading us to propose that the diffusion of the IFT kinesin motor may, itself, be the long-sought length sensor that regulates IFT injection. The complicating factor in such a model is that the source of the diffusing molecule, kinesin, is itself dependent on the rate of injection, which in turn is dependent on the rate of diffusive return. This mutual feedback between injection and return raises the question of whether such a system is capable of stably achieving a unique length at steady state. It is also not obvious how this type of system will perform when two flagella are considered simultaneously.

In this paper, we investigate this hypothesis using a fine-grained agent-based model that is analyzed using computer simulations together with a coarse-grained differential equation model that can be solved analytically. In the agent-based model, we explicitly model the flagellum and motors and run time dynamics simulations. In the differential equations model, we solve the steady state form of the diffusion equation with boundary conditions that incorporate active delivery of IFT to the tip and diffusive return to the base. Each model is detailed below. The result of our analysis is that diffusive return of kinesin, when combined with a simple model for IFT-mediated flagellar assembly, does indeed predict a stable flagellar length control system

capable of achieving a unique steady state length and of equalizing the lengths of flagella in a biflagellate cell, without the need to add any additional components beyond what is already known from prior studies of IFT.

2. Agent-Based Model

As a starting point to look for potential length dependencies in the IFT system, we implemented a simplified model of the individual components of the system (Figure 1.1B) and asked what predictions this model might make about length dependence. We built an agent-based model to simulate kinesin and microtubule growth dynamics through stochastic rules grounded in biochemistry. Specifically, we used Python's built-in object oriented programming methods to explicitly model individual motors and the flagellum they populate.

The flagellum has attributes including length and environmental variables including decay rate and diffusion coefficient. Each motor has attributes including position, transport speed, a Boolean to indicate whether it is in the flagellum or in the base, and another Boolean to indicate whether it is bound (in active transport) or unbound (diffusing) if it is in the flagellum. To simulate dynamics, we cycle through each motor and test a series of conditionals to determine how it should adjust its position. If it is on the flagellum and bound, its position increases by a constant. If its position reaches the flagellum's length, indicating that it has reached the tip of the flagellum, it unbinds (changes its state from active transport to diffusion), and the flagellum grows by the designated growth increment. If it is in the flagellum and unbound, it moves randomly to the left or to the right. If it is unbound and reaches the base, it is absorbed into the base and becomes inactive. At each time step, we count the number of motors in the base, and if that value is greater than a variable for avalanche threshold, we use a Weibull distribution to determine how many avalanche out and move into the flagellum, and reactivate into active

transport. We chose a Weibull distribution because it can fit the long-tailed distribution of train sizes that have been experimentally determined (16). The Weibull distribution has a multiplicative constant that we set to the difference between the number of motors in the base and the threshold for avalanching, plus a constant we could vary. Meanwhile, at each time step, the flagellum shrinks by the decay rate constant. Table 1 lists parameters we used, and how we obtained the values used for simulation.

It is important to note that this model does not specifically represent the IFT particles. It is assumed that each motor is associated with an IFT particle carrying a fixed quantity of material, as represented by the growth size per motor.

This model lets us consider the journey of a single motor (Fig. 1.2A). In the example shown, it starts in active transport at position 0. The conditional that checks if it is bound commands its position to increase by the active transport step size. This process continues until the position of the motor is equal to the length of the flagellum. This position represents the tip, and at this stage, the motor's bound parameter is changed to False (representing diffusion), and the length of the flagellum is increased by the build size parameter. In the next time step, the conditional that checks if the motor is bound sees that it is not bound, and this time it adjusts its position by the root mean square diffusion length multiplied by either 1 or -1, determined randomly. This simulates the randomness of diffusion. Once its position reaches 0 (the base), its Boolean value stating whether it is in the flagellum is set to False to indicate absorption to the basal pool. Every time step, a random power law number generator determines how many motors that are inactive at the base are injected onto the flagellum. If that number is zero, or if it is nonzero but this motor is not among those injected, this motor will stay stationary at position zero. Once it gets injected, it goes back into the flagellum in active transport, and the entire

process repeats for the remainder of the simulation. By simulating many motors within the same flagellum, each adding length to the flagellum upon reaching the tip and then diffusing back, combined with constant shortening of the flagellum, we can simulate the overall growth dynamics of a single flagellum, as shown in figure 1.2B. Simulations over time show that this system allows the flagellum to grow to a defined length with decelerating kinetics.

Because motors undergo random motion as they return, and are released from the base in a way that depends on the time history of their return, it is expected that flagellar growth rates will fluctuate, and indeed our simulations confirm that the length does indeed fluctuate around a steady state average length. We found that the magnitude of this fluctuation varied between simulated flagella with different parameter values even if they reach the same steady-state length (Fig. 1.2C), indicating that fluctuation contains additional information about the system beyond what the steady-state length provides. By counting motors in different states, we can ask how the pool of diffusing motors is distributed along the length. We find that the probability of finding a motor at a given distance from the tip is approximately linear, consistent with the expected form of a diffusional gradient at steady state (Fig. 1.2D).

Having found that the simple agent-based model of diffusive kinesin return is able to produce a defined flagellar length, the key question is whether the length-dependence of IFT injection can be recapitulated. As shown in Figure 1.2E, the average injection size per unit time of injected IFT trains in the simulation shows an inverse dependence on flagellar length, as previously reported in experimental measurements (16, 17).

The length control system modeled here is stable, as indicated by simulated experiments in which the length is transiently perturbed. As illustrated in Figure 1.2F, a transient externally imposed elongation of a flagellum at steady state, achieved by simply resetting the length to a

longer value, is followed by a shortening back to the steady state length. This implies that the steady state length is determined by the input parameters rather than the transient state of the flagellum.

3. Dependence of length on model parameters

The agent-based model described above is a minimalist representation of the IFT system, but while our simulations show that stable length is achieved, it is not obvious from the successful simulations why the model works or how the parameters of the model contribute to the value of the steady state length. In order to gain a physical understanding of how this model achieves length control, we investigated a more idealized model that will allow us to solve for the steady state solution analytically. By reducing the model a to classical boundary value problem, we can solve for system behavior as a function of key parameters in closed form. If we make the assumption that active transport time and expected time delay of injection is small relative to the timescale of diffusive return, we can model this system as a diffusion problem with a constant source of free motor protein at the tip of the flagellum and a sink at the base. If we also assume that no diffusing motors re-bind to the flagellum, we can apply Fick's first law of diffusive flux in steady state. This law strictly applies to steady state, however we can still use it to study the dynamics of flagellar growth by invoking a separation of timescales. We assume that the timescale of flagellar length changes due to growth and shrinkage, which happens on the timescale of minutes to hours, is slow relative to the timescale over which diffusion establishes a stable gradient, such that the system can be viewed as being in a quasi-steady state. (This similar to the classic statistical mechanics problem of slowly expanding a box containing gas: when the expansion of the box is slow, the system is reversible and equilibrium statistical mechanics

theory can be applied. A simple validation of this is that a single motor reaching the tip increases the length by 1.25nm in our simulation with default parameters, and it takes 4.5 nanoseconds for a diffusing motor's mean square displacement to equal 1.25nm, which is negligible compared to the roughly 18 seconds it takes to diffuse back to the base).

The strategy for deriving an expression for steady state length is to determine the expected flux of diffusing motors arriving at the base, equate the flux to the number of motors diffusing from the tip (following our assumptions that injection time and active transport time are very small compared to diffusion time), convert that flux into a dynamic growth term, and then find the steady state at which this growth is balanced with the decay term.

The resulting expression for steady state length is the following:

$$L_{ss} = \left(\frac{2ND\delta L}{d}\right)^{\frac{1}{2}}, \qquad (1.1)$$

where N is the number of diffusing motors, D is the diffusion coefficient, δL is the increment of flagellar growth when a motor reaches the tip, and d is the decay rate. The derivation is below.

The time it takes a random walker to move a root mean square distance L is:

$$t = \frac{L^2}{2D}.$$

The current of motors I reaching the base is equal to the number of diffusing motors N divided by the average time it takes to diffuse to the base.

$$I = \frac{N}{t} = \frac{2ND}{L^2}.$$

In the approximation in which motors that have reached the base immediately transport back to the tip, the flagellum grows at a rate given by the current of motors reaching the base multiplied by the growth increment per motor δL. The competing decay term d is length-independent.

$$\frac{dL}{dt} = \frac{2ND\delta L}{L^2} - d.$$

At steady state, $\frac{dL}{dt} = 0$, so we can solve for the steady-state length L_{ss}.

$$L_{ss} = \left(\frac{2ND\delta L}{d}\right)^{\frac{1}{2}}.$$

An identical result can be obtained by solving the diffusion equation for appropriate boundary conditions and expressing the motor return rate in terms of the flux at steady state.

This model predicts that the steady-state length of the flagellum is proportional to the square root of its diffusion coefficient, motor number, and unit length increase per motor. It also predicts that steady-state length is inversely proportional to the square root of the decay rate. Note that since the model proposed does not invoke any unknown transducer molecules or pathways, but instead directly represents all of the molecular players, there is no need for any undetermined constant of proportionality.

By running simulations in the agent-based model over a range of parameters, we can verify that this relation matches the results of fine-grained agent based simulations (Fig 1.3). Specifically, we see close matches between theory and simulation as we vary diffusion coefficient (Fig 1.3A), number of motors (Fig 1.3B), length increase per motor (Fig 1.3C), and decay rate (Fig 1.3D). When simulated lengths are plotted versus the prediction of equation (1.1), we observe a virtually identical match (Fig 1.3E), with < 5% deviation on average. This is also true when parameters are varied in combination (Fig 1.3F). To simulate our assumptions, these simulations have an avalanching threshold of 1 motor and an active transport speed of 200 μm/s (enough to go the entire length of the flagellum in one time step). The similarity between the predictions of equation 1.1 and the simulated lengths indicate that equation 1.1 accurately describes the length of diffusion-regulated flagella. For all parameter combinations simulated, a

single steady-state length is achieved. We used a Markov model to verify that the presence of a unique stable steady state solution is intrinsic to the model (see Supplemental Figure S1.1).

Equation 1.1 above describes the steady state flagellar length in the limit of instantaneous injection and active transport. To determine whether deviations from these assumptions might have a significant effect over a large region of parameter space, we simulated flagella with a wide range of the parameters not included in equation 1.1. Specifically, we scanned over IFT velocity and avalanching parameters and held all other parameters constant. The effects on steady-state length are displayed in figure 1.4. The Weibull distribution used to determine avalanching dynamics has two parameters: the power and the prefactor. Figure 1.4A shows the final lengths generated by varying the power, and figure 1.4B shows the finals lengths generated by varying the prefactor. Both indicate that the Weibull parameters do not significantly affect length, implying that the specifics of IFT injection do not affect final length. This can be understood by considering that the avalanching dynamics dictate that on average, larger injections lead to more time between injections. So in steady state, the average build rate of the flagella is independent of avalanching parameters. The avalanching threshold (Fig 1.4C) affects the final length because increasing the threshold increases the average number of motors in the base at any given time, thereby decreasing the number of diffusing motors and decreasing the steady state length. Essentially,

$$N_{flagellum} = N - N_{thresh}. \quad (1.2)$$

The velocity of motors only affects the final length in low velocity regimes (Fig 1.4D). This is also due to the effective decrease in motors in diffusion. The number of motors in active transport, diffusion, and the base combined is conserved, so the longer a motor is in active transport or waiting at the base, the less often it is diffusing. To calculate the fraction of motors

inside the flagellum in diffusion, we must consider the time it takes to complete active transport and diffusion, and treat this as the probability of drawing a diffusing motor. The time it takes for a particle to diffuse a root mean square distance L is $L^2/(2D)$, and the time it takes for a motor with constant speed v to move a distance L is L/v. The sum of these two is the mean total time to complete active transport and diffusion, so the probability of drawing a diffusing motor is

$$p_{diffusing} = \frac{\frac{L^2}{2D}}{\frac{L}{v}+\frac{L^2}{2D}},$$

which simplifies to

$$p_{diffusing} = \frac{1}{1+\frac{2D}{Lv}}, \qquad (1.3).$$

To confirm the relations in equations 1.2 and 1.3, we superimposed the curves onto figures 1.4C and 1.4D, respectively. The low root mean square residuals to these curves shows that these corrective terms adequately describe the changes in length associated with avalanching threshold and transport velocity. Combining equations 1.2 and 1.3 yields an overall correction for the N used previously for the number of motors used to predict steady state length:

$$N_{eff} = (N - N_{thresh})\left(\frac{1}{1+\frac{2D}{Lv}}\right), \qquad (1.4)$$

where N_{eff} is the effective number of motors, the number of motors in diffusion.

Figure 1.4E shows the steady state length in simulations with random values for velocity and avalanching threshold. The predicted length values are generated using equation 1.1 with the value for N_{eff} plugged in for N. Note that the final length is included in the expression for N_{eff}, so we used the final length from the simulation in the expression for the prediction instead of solving for L directly, since our goal is just to show the validity of the equation.

4. Coordination of multiple flagella

The model as it stands only includes a single flagellum, whereas Chlamydomonas cells have two. Experimental evidence shows that the two flagella in a given cell interact. Indeed, one of the most dramatic experiments in the length control literature is the demonstration that cells can equalize the lengths of their two flagella after one has been cut (called the "long-zero" experiment) (2). This is crucial for swimming, but more importantly, it creates the striking visual impression that each flagellum "knows" how long the other one is. In models that involve length sensor pathways, this coordination can be explained by some sort of molecular cross-talk between the length sensing pathways. In the diffusion-based length control model described here, there is no length-sensing pathway per se, and instead length influences growth rates simply by the timescale of diffusive return. This raises the question of whether the model can account for length equalization.

To answer this question, we expanded the model to simulate two flagella competing for a common pool of material (Fig 1.5). We imagine the material in question to be tubulin, but in fact the axoneme is a complex structure with many proteins in it, some of which are involved in its assembly, and we do not currently know which axonemal structural protein is the limiting factor in terms of flagellar length. To include the effect of pool depletion in our model, we changed the amount that the flagellum grows when a motor reaches the tip from a constant to a proportion of the size of the free pool. For a total pool size T, flagellar lengths L_1 and L_2, and a constant of proportionality k_{pool}, the build size of an injected motor becomes

$$\partial L = k_{pool}(T - L_1 - L_2) \qquad (5)$$

Note that we express the size of the pool T in units of length, so the pool can be thought of as the maximum possible total flagellar length. In the early growth phase, L_1 and L_2 are small, so the build size of an injected motor is big (Fig 1.5A). Later, the flagella are longer, so the smaller amount of available material leads to a smaller build size (Fig 1.5B). Note that the building material does not have to be fully depleted for the flagella to stop growing, since the kinesin availability is still in competition with the constant decay.

Figure 1.6 shows the results of the new simulation. To simulate the long-zero experiment, we simulated a two-flagella cell until it reached steady state then set the length of one flagellum to zero (Fig 1.6A). The length of the cut flagellum was subtracted from the total pool size, since the flagellar material gets lost after being cut. At this stage, we increased the pool size slowly over time until it returned to its original value. The cut flagellum then grows as the long flagellum shrinks. Once they reach the same length, they grow together to steady state. This is consistent with experimental long-zero dynamics. We have a new prediction for final length by replacing the constant ∂L in equation 1.1 with the pool size-dependent expression in equation 1.5.

$$L_{ss} = \left(\frac{2N_{eff}Dk_{pool}(T-2L_{ss})}{d}\right)^{\frac{1}{2}} \qquad (1.6)$$

Note that in steady state, $L_1 = L_2 = L_{ss}$.

We validated the equation by simulating over a wide range of parameters and comparing the two sides of the equation (Fig 1.6B). Since L_{ss} is in both sides of equation 1.6, we plotted the two sides of the equation against each other. On average, there is < 5% deviation between the

two sides of the equation, indicating that equation 1.6 accurately describes the steady-state lengths of two diffusion-regulated flagella competing for a common pool of material.

The effect of *T* on the steady state length depends on the relative size of *T* compared to the other parameters. In regimes with low *T* compared to the ratio of build terms and decay terms, the common pool is limiting, and the final flagellar lengths will approach *T/2*. In the opposite regime, with high *T*, kinesin remains the limiting factor, and the only effect of T is the steady state build size.

5. Discussion

5.1 Diffusion as a ruler

In this model of length sensing, the cell does not employ a sensor, such as the molecular rulers used for bacteriophage tail length, but rather harnesses the fact that the time scale of diffusion is a function of the distance over which a particle must diffuse. This model is similar to a chemical reaction in which a chemical X has an assembly term and a degradation term. The concentration of X over time is given by a simple differential equation, and the steady state concentration is determined by a combination of biochemical parameters. The flagellum is a similar system because the length has assembly and disassembly terms, and here we predict which specific biochemical parameters are involved (equation 1.1). There is a competition between a growth flux term ($\delta L * N * D$) and a decay term d. Two of these parameters, δL and N, implicitly contain additional meaningful parameters such as active transport velocity, avalanching threshold, and the size of the shared pool of material (equation 1.6). It is important to note that the square root in equation 1.1 comes from the geometry of the system.

We (19) and others (24) have previously noted that diffusive movement of a signal from one end of the flagellum to the other could be used as a length-measuring scheme. However these prior models always invoked a "black box" in the form of some machinery that responds to the signal to alter flagellar dynamics. For example, our previous models (19) invoked the idea of a flagellar gate or pore whose opening was regulated by the diffusible signal. Because the nature of this black box was not known, for example its input-output relation, it was not possible to confidently make predictions to be compared with experiments. Our model described here avoids the need for any unspecified black boxes, because the kinesin motor that drives IFT is, itself, the diffusing entity. This allows the parameters of our model to be directly related to experimental predictions. For example, equation 1.6 can be used to determine how variation in different experimentally accessible parameters should alter length.

5.2 Relating model to genetics of length control

The simple mechanism modeled here is sufficient to explain length-dependent IFT injection and stable length control without needing to invoke any new molecular players beyond those already known. But this does not mean that the model works independently of molecular entities. All of the model parameters are determined by the biophysical and enzymatic properties of the known molecular component of the IFT system. It is to be expected that mutations in these molecules can alter flagellar length in predictable ways, potentially allowing the model to help interpret the mechanistic basis of previously described flagellar length-altering mutants.

The diffusion constant of kinesin is mainly a property of the size of the molecule and the viscosity of the flagellar matrix, and is thus unlikely to be dramatically altered with point mutations. But it is not hard to imagine that mutations might alter the dynamics of the injection

system at the base. Previous research shows that the *lf4* mutant makes the flagellum longer and increases the injection rate but without eliminating the length dependence of injection (16). Such a phenotype could correspond to lowering the threshold of motor buildup required for injection avalanching, which is a parameter in the agent-based model. High thresholds lead to lower injection frequency and lower steady state length, and low thresholds lead to higher injection frequency and higher steady-state length, as shown in the correction for N in equation 1.4 and its effect on steady-state length (eq. 1.6). This implies that it is possible that the LF4 gene controls the threshold for how big the pile can be before an avalanche occurs.

Another mutant that we can examine is the FLA10 gene, which codes for the kinesin motors (9). Temperature-sensitive *fla10* mutants with intact flagella start to lose their flagella when the temperature shifts into the region that disables FLA10 (9). Growth of *fla10* mutants at intermediate temperatures, which partially disable the motors, leads to intermediate steady-state flagellar lengths (11). In our model, this translates to a reduction in N, the number of motors in the system. We note that the square-root dependence of steady state length on motor number (equation 1.1) means that length will decrease sub-linearly with decreasing motor number. To reduce length by a factor of 10 would require a reduction in motor number by a factor of 100. Thus, one prediction of this model is that the quantity of motors can be partially depleted, for example in the *fla10* mutation at permissive temperature, and have little detectable effect on length.

5.3 Comparison with other studies

A recent study on mouse axons (23) studies the diffusion of kinesin motors as a mechanism for recycling. Their model for simple diffusion has the same linear distribution of

diffusing motors, but they find that the diffusing motors have a nonzero binding rate onto the flagellum from diffusion, and therefore the number distribution is exponential. The mouse axon system has a fixed length, but their work provides an example in biology of diffusion and recycling of kinesin.

Models based on diffusion as a length measurement system have been proposed by Levy (24) and by Ludington (16, 19). In the model by Levy, the proposed source of the diffusing molecule was the base, not the tip, and it was assumed that the diffusing species directly affected assembly, as opposed to our model in which the diffusing molecule affects transport. In the Ludington 2013 model, RanGTP was the diffusing substance, and the link to injection was indirect, requiring a gating of entry by activated Ran (16). In the diffusion model investigated in Ludington 2015, the identity of the diffusing molecule was not specified and again a transducer system was assumed to couple the diffusive molecule to the injection system (19). Finally, we note that while a strength of our model is that length can be sensed and converted into length-dependent IFT injection without the need to invoke any other molecular players, it has been shown that kinases inside the flagellar compartment do show length-dependent activity (25, 26). Likewise, flagellar disassembly can become length dependent when flagella grow outside of a normal length range (27). It is interesting to consider whether these molecular activities may be dependent on IFT injection or diffusive return.

5.4 Future Prospects

A fundamental puzzle of flagellar length control has always been how a molecular signal could be generated that depends on length. Our prior results indicated that IFT injection was length dependent but did not explain the origin of the length dependence, thus raising the

possibility that some complex length-measuring molecular pathway may exist. The results presented above establish that diffusive return of kinesin motors is, at least in principle, capable of providing a length measurement system for regulating IFT injection as a function of flagellar length, without requiring any additional regulatory or sensing components. In other words, the IFT system may contain its own measurement method based on the physics of diffusion. It is interesting to consider whether this type of measuring system could be at work in other linear cellular structures such as microvilli or microtubules.

Author Contributions

N.H. wrote the simulations. N.H., M.T., and W.M. developed ideas and worked out math. N.H. and W.M. wrote the manuscript.

Acknowledgments

We would like to thank Greyson Lewis for help with the math and derivations and Ahmet Yildiz for sharing results ahead of publication. This work was supported by NIH grant GM097017.

Code Availability

Code for agent-based simulations and Markov matrix simulations is available at https://github.com/nathendel/Hendel-et-al-2017.

Table 1.1.

Parameter	**Default value**	**How value was obtained**
Number of motors	200	Marshall et al, 2001 (11)
Active transport speed	2 um/s	Chien et al., 2017 (22)
Growth size per motor	1.25 nm	Marshall et al., 2001 (11)
Decay rate	0.01μm/s	Marshall et al., 2001 (11)
Diffusion coefficient	1.75 $\mu m^2/s$	Chien et al., 2017 (22)
Weibull distribution power	2.85	Ludington et al., 2013 (16)
Weibull distribution prefactor	10	Arbitrary
Avalanche threshold	30 motors	Ludington et al., 2013 (16)

Figures

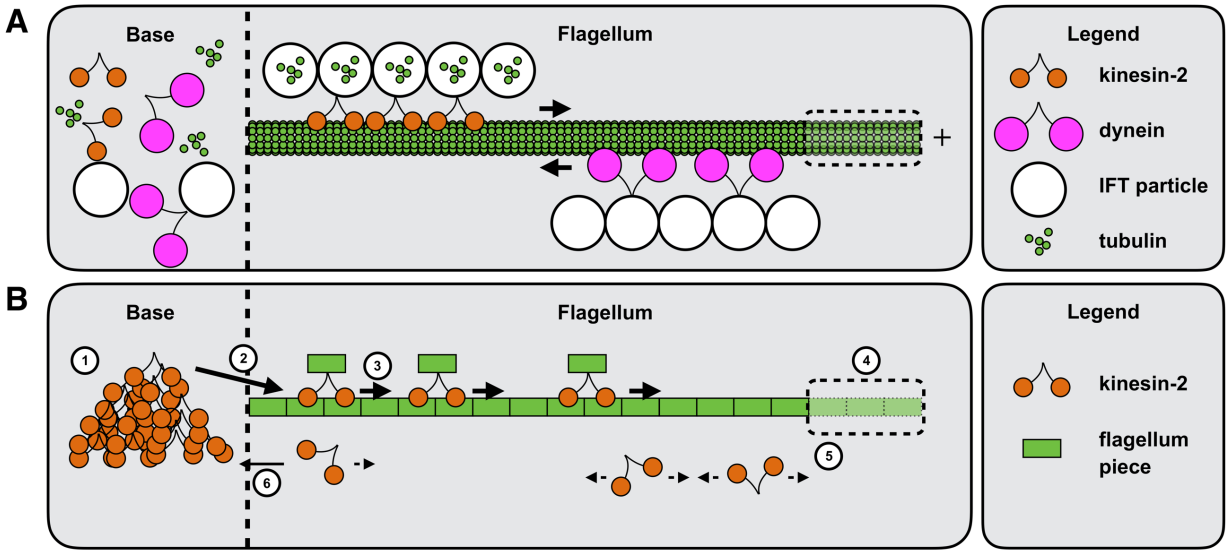

Figure 1.1. Agent-based model of IFT
(A) Diagram of IFT. Kinesin-2 motors form trains that carry IFT particles containing tubulin to the plus end of the microtubule bundle, the tip of the flagellum. Dynein motors carry the IFT particles back to the base. (B) Model version of IFT. Kinesin motors pile up at the base (1), and once the pile is large enough, some are injected into the flagellum with cargo (2). Each motor constantly moves towards the tip of the flagellum (3). Once they reach the end, they flagellum gets longer (4), and the kinesin motors unbind and diffuse (5). Once they diffuse back to the base, they are absorbed and re-enter the pile in the base (6). While this is happening, the flagellum is shrinking at a length-independent rate.

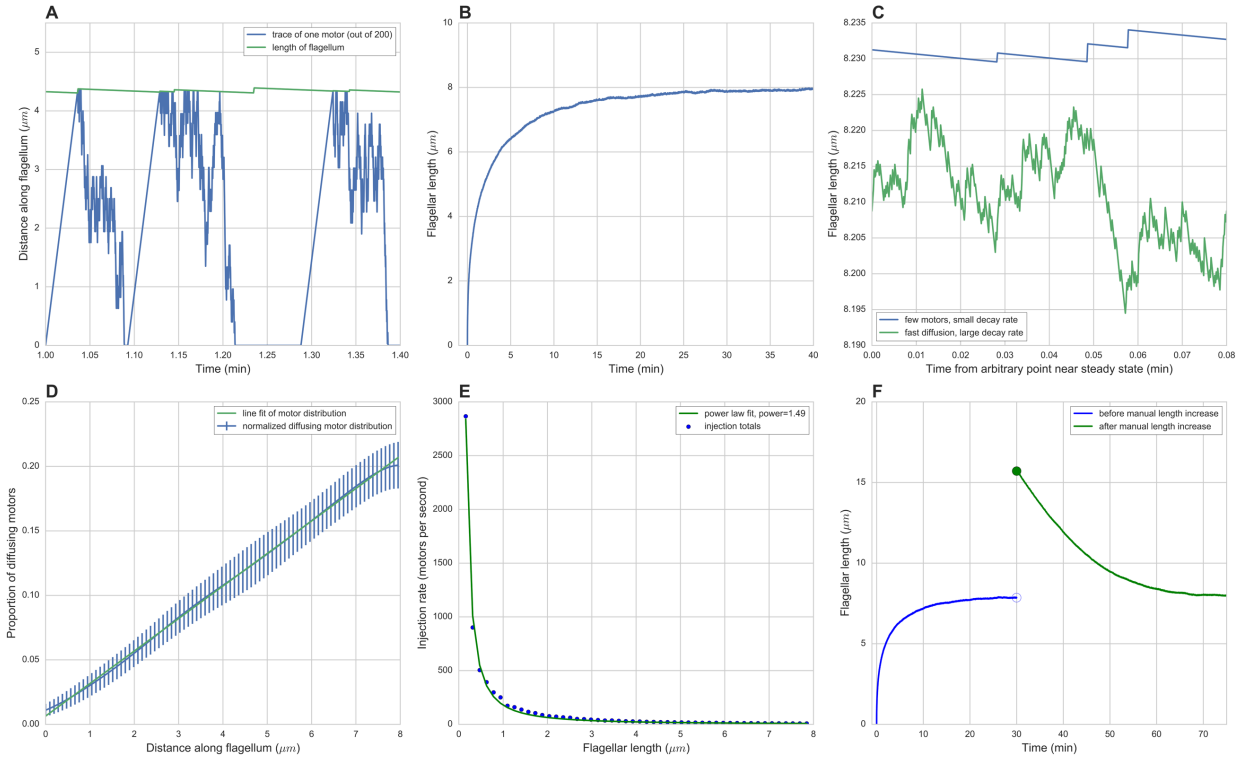

Figure 1.2. Results of agent-based simulation
(A) (Blue) journey of a single motor in a zoomed-in window of the flagellum's early growth, (green) flagellar length. (B) Flagellar length over time in simulated minutes. (C) Expanded window of two simulated flagella's lengths over time as they approach steady state. The blue trace is for a flagellum with a small number of motors and a small decay rate, and the green trace is for a flagellum with a larger number of motors, larger diffusion coefficient, and larger decay rate. The standard deviation of the blue trace is 1.40e-3 μm, the standard deviation of the green trace is 6.69e-3 μm in the time frame shown. (D) (Blue) Distribution of diffusing motors along flagellum using the average of 103 simulations with identical parameters and a Gaussian kernel density function applied to the means at each position, (green) linear fit. (E) Plot of injection size as a function of flagellar length. The points were generated by simulating 10 cells, taking their injection times and sizes, and binning them into measurements of average injection size per unit time in each of the 50 evenly-spaced bins. (F) Stability of length control system. Plot shows simulation in which length was manually increased to double its steady state length at t=30 min. (Blue) is before the manual increase, (green) is after, showing restoration to initial steady state length. The time step in each simulation was 0.01 seconds.

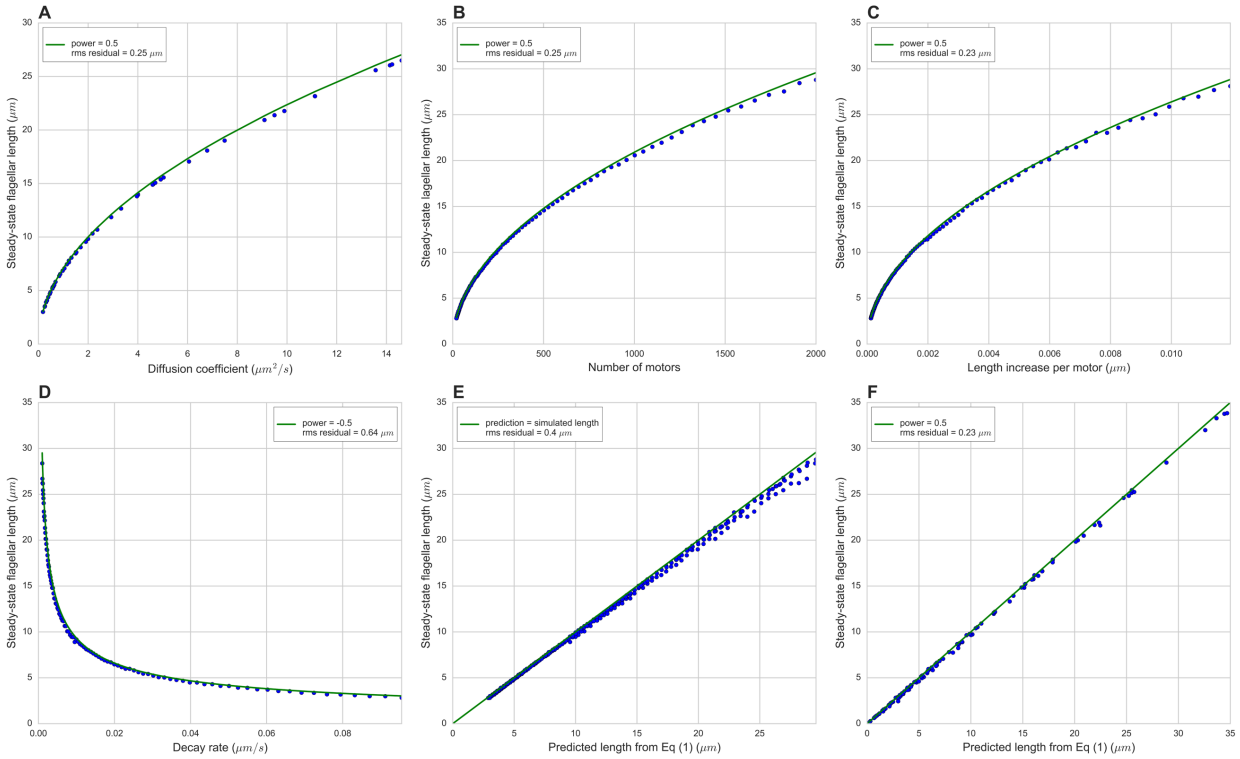

Figure 1.3. Comparison of analytical solution of diffusion equation to agent-based model
Each plot shows the steady-state lengths given by equation 1.1 and agent-based simulations by varying a single parameter at a time. The varied parameters are: (A) diffusion coefficient D, (B) number of motors N, (C) length increase per motor δL, (D) decay rate d, (E) plot of length predicted from equation 1.1 compared to simulation results. In this panel, all individual parameter variation simulated in the plots from panels A, B, C, and E are plotted in the same graph, with the parameter set used in each simulation inserted into equation 1.1 to yield the predicted length, then plotted against the final steady-state length simulated by the agent-based model. (F) Simulated steady-state lengths of flagella with randomly selected values for D, N, δL, and d. In this panel, all four variables were simultaneously varied, instead of varied individually as in panel E. Each subplot has the curve predicted from equation 1.1 superimposed onto the data in green, along with a root mean square value for the residual between the simulated lengths and the prediction. The points in all panels were uniformly sampled in log space, so there are the same number of points between the default and one order of magnitude below as there are between the default and one order of magnitude above.

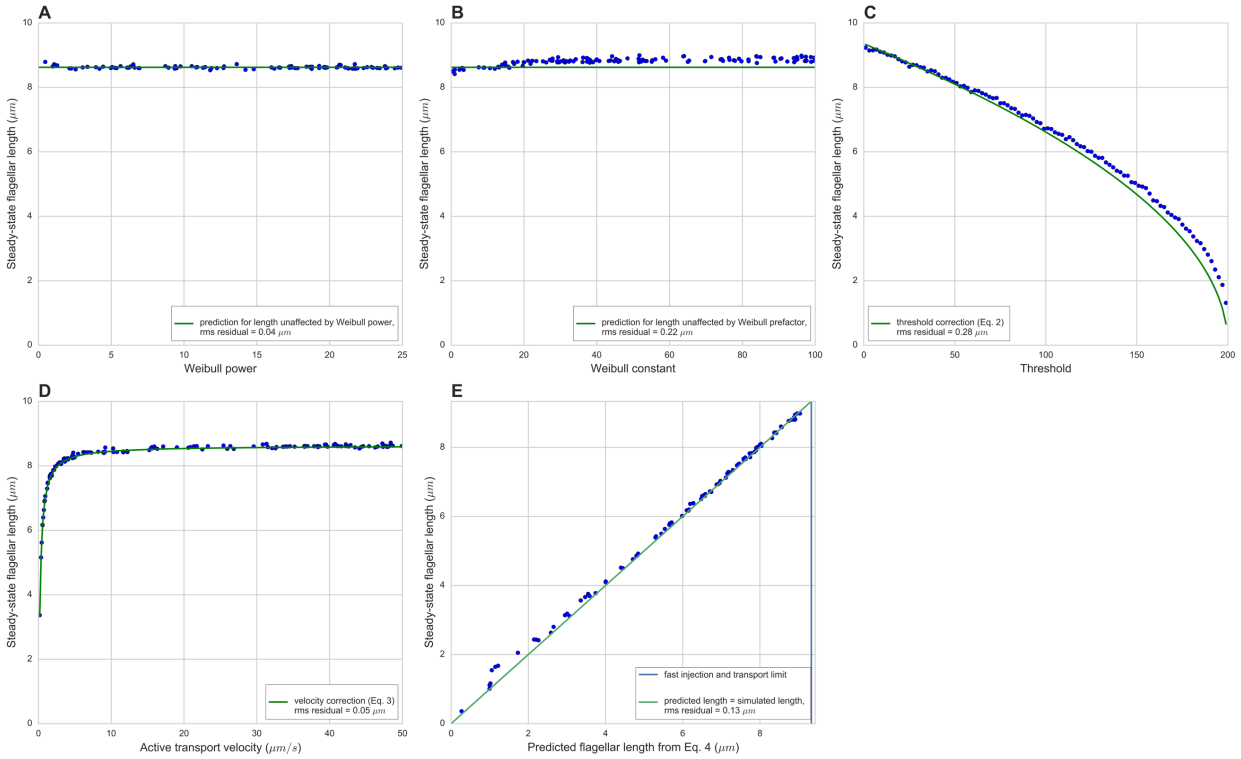

Figure 1.4. Effect of remaining parameters on steady-state length
Each plot shows the steady-state lengths for simulations altering variables not included in equation 1.1. The varied parameters are: (A) Weibull distribution power, (B) Weibull distribution prefactor, (C) avalanching threshold (number of motors built up in the base required to trigger an avalanche), and (D) velocity of motors in active transport of IFT. The varied parameters in (A)-(C) are involving in the avalanching mechanism. Each panel has a line in green superimposed on the data representing the effect that variable has on steady-state length. In (A) and (B), we claim there is no significant effect. In (C), equation 1.2 is superimposed on the simulated data, and panel (D) has equation 1.3 superimposed. In (E), the threshold and transport velocity are both randomly generated and simulated, and equation 1.4 is superimposed. Root mean square residuals between the simulated lengths and the predictions are displayed in the legends of each panel.

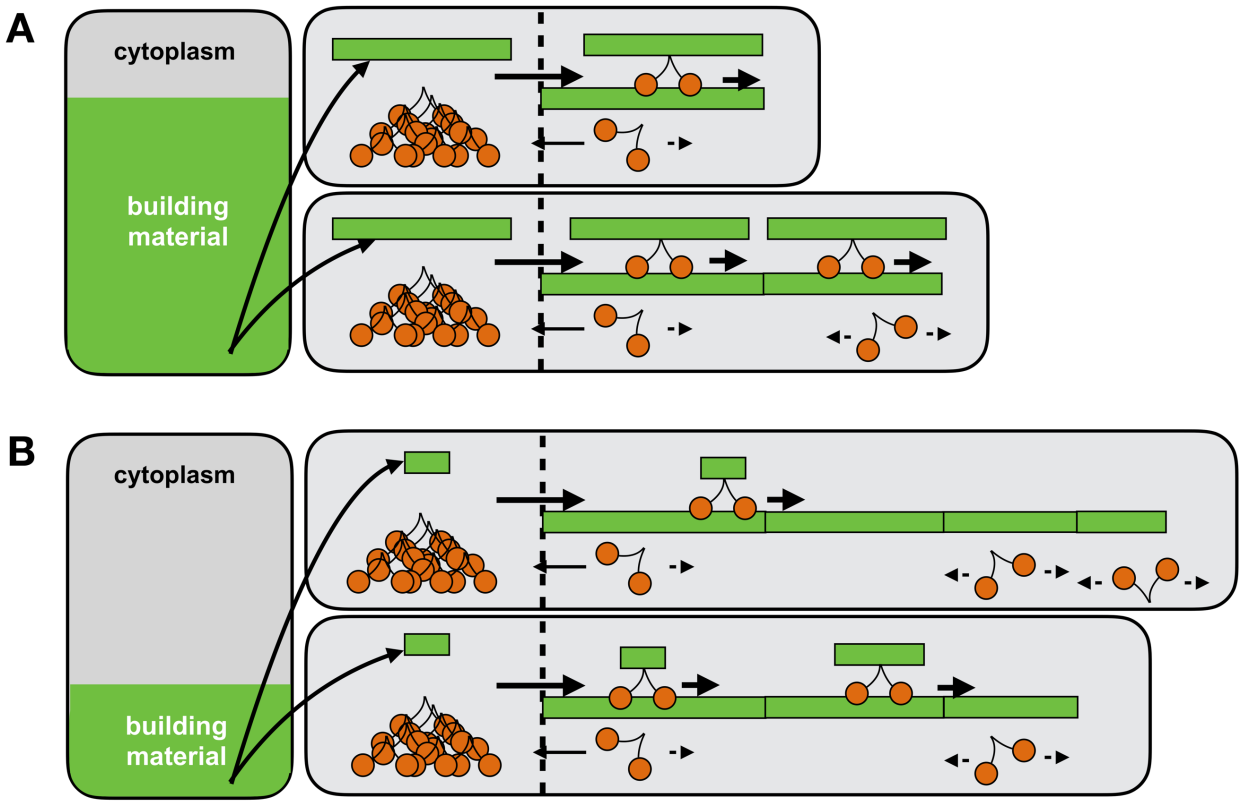

Figure 1.5. Two-flagella model
Diagram of model expanded to include a second flagellum and a shared pool of material. The amount of building material each motor carries is proportional to the remaining amount of shared material in the pool (Eq. 1.5). (A) Early on in the growth of the flagella, the amount of material is high, and therefore the amount of building material each motor carries is high. (B) Later in the growth of the flagella, the material pool has been partially depleted to build the flagella, so the build size per motor has decreased.

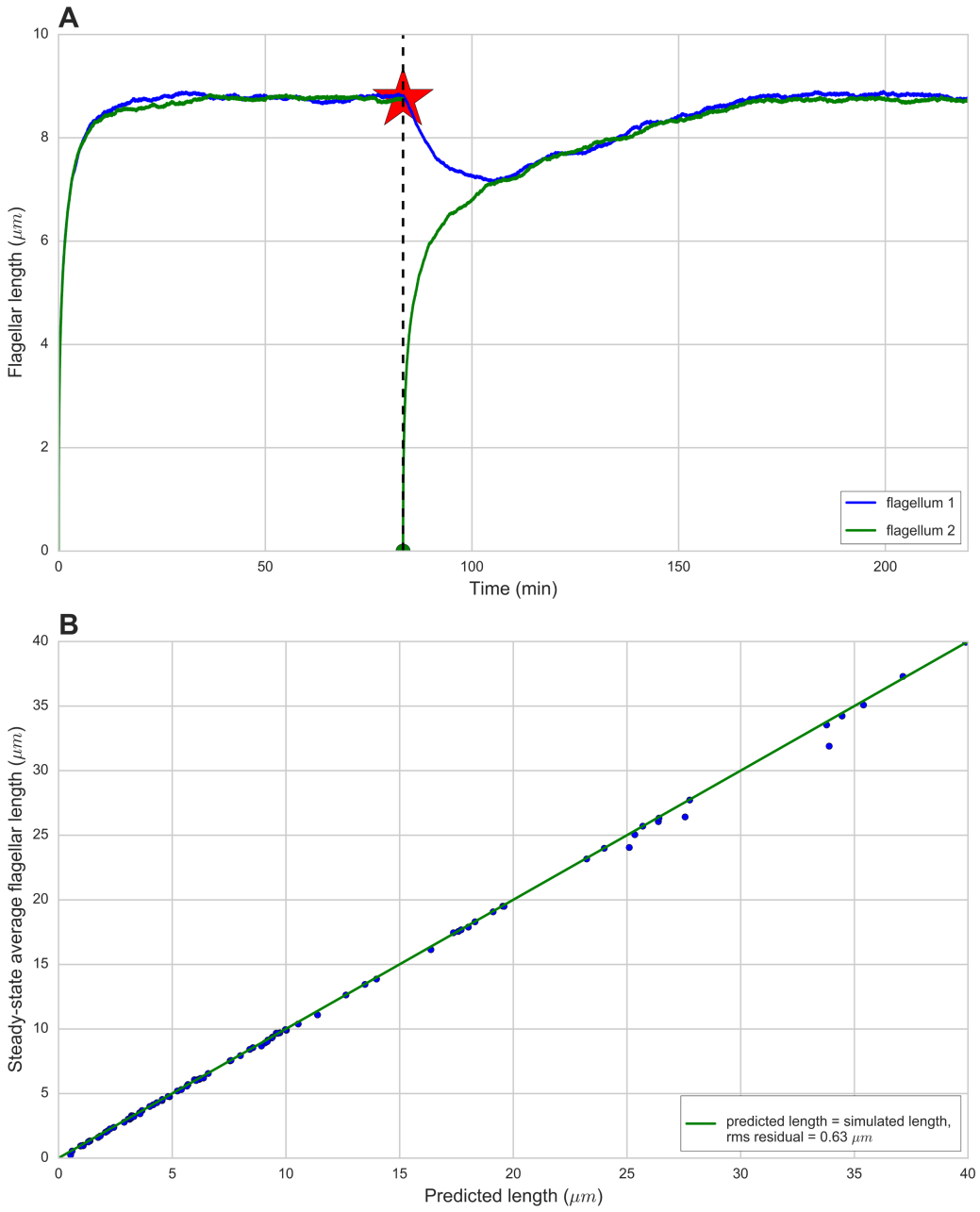

Figure 1.6. Simulation with expanded two-flagellum model
(A) Length over time plots for simulation of two flagella competing for a common pool of material. At the time point indicated by the red star, we manually set the length of flagellum traced in green to zero and subtracted its prior length from the pool size. We then resumed the simulation, slowly increasing the pool size until it reached its original value. This is a simulation of the "long-zero" experiment. (B) Comparing the prediction of equation 1.6 to the simulated length. Since the right hand side of equation 1.6 includes L, we plotted the left hand side of eq. (1.6) on the y-axis and the right hand side on the x-axis. The values for steady-state length were calculated by averaging the steady-state lengths of the two flagella. The green line superimposed onto the data is y = x, showing where the two sides of equation 1.6 are equal.

References

1. Mohapatra L, Lagny TJ, Harbage D, Jelenkovic PR, Kondev J. 2016. Length control of filamentous structures in cells by the limiting pool mechanism. bioRxiv doi.org/10.1101/075655
2. Rosenbaum, J.L., Moulder, J.E., and Ringo, D.L. 1969. Flagellar elongation and shortening in *Chlamydomonas*. The use of cycloheximide and colchicine to study the synthesis and assembly of flagellar proteins. *J. Cell Biol.* 41: 600-19
3. Cole, D., Diener, D., Himelblau, A., Beech, P., Fuster, J., and Rosenbaum, J. (1998). Chlamydomonas kinesin-II–dependent intraflagellar transport (IFT): IFT particles contain proteins required for ciliary assembly in Caenorhabditis elegans sensory neurons. The Journal of Cell Biology *141*, 993.
4. Scholey JM. 2003. Intraflagellar transport. *Ann. Rev. Cell Dev. Biol*. 19: 423-43.
5. Taschner M, Lorentzen E. 2016. The intraflagellar transport machinery. Cold Spring Harvor Perspect. Biol. 8, a028092.
6. Lechtreck KF, van de Weghe, JC, Harris JA, Liu P. 2017. Protein transport in growing and steady-state cilia. Traffic 18, 277-286
7. Stepanek L, Pigino G. 2016. Microtubule doublets are double-track railways for intraflagellar transport trains. Science 352, 721-4.
8. Vannuccini E, Paccagnini E, Cantele F, Gentile M, Dini D, Fino F, Diener D, Mencarelli C, Lupetti P. 2016. Two clases of short intraflagellar transport train with different 3D structures are present in Chlamydomonas flagella. 129, 2064-74.
9. Kozminski KG, Beech PL, Rosenbaum JL. 1995. The Chlamydomonas kinesin-like protein FLA10 is involved in motility associated with the flagellar membrane. *J. Cell Biol.* 131: 1517-27.

10. Mueller J, Perrone CA, Bower R, Cole DG, Porter ME. 2005. The *FLA3* KAP subunit is required for localization of kinesin-2 to the site of flagellar assembly and processive anterograde intraflagellar transport. *Mol. Biol. Cell* 16: 1341-1354.

11. Marshall, W.F., and Rosenbaum, J.L. 2001. Intraflagellar transport balances continuous turnover of outer doublet microtubules: implications for flagellar length control. *J. Cell Biol.* 155: 405-414.

12. Marshall, W.F., Qin, H., Rodrigo Brenni, M., and Rosenbaum, J.L. 2005. Flagellar length control system: testing a simple model based on intraflagellar transport and turnover. *Mol. Biol. Cell* 16: 270-278.

13. Deane, J.A., Cole, D.G., Seeley, E.S., Diener, D.R., and Rosenbaum, J.L. (2001). Localization of intraflagellar transport protein IFT52 identifies basal body transitional fibers as the docking site for IFT particles. Curr Biol *11*, 1586-1590.

14. Dishinger, J.F., Kee, H.L., Jenkins, P.M., Fan, S., Hurd, T.W., Hammond, J.W., Truong, Y.N.-T., Margolis, B., Martens, J.R., and Verhey, K.J. (2010). Ciliary entry of the kinesin-2 motor KIF17 is regulated by importin-beta2 and RanGTP. Nat Cell Biol *12*, 703-710.

15. Hu, Q., Milenkovic, L., Jin, H., Scott, M.P., Nachury, M.V., Spiliotis, E.T., and Nelson, W.J. (2010). A septin diffusion barrier at the base of the primary cilium maintains ciliary membrane protein distribution. Science *329*, 436-439.

16. Ludington WB, Wemmer KA, Lechtreck KF, Witman GB, Marshall WF. 2013. Avalanche-like behavior in ciliary import. *Proc. Natl. Acad. Sci. U.S.A.* 110: 3925-30.

17. Engel, B.D,. Ludington, W.B., and Marshall, W.F. 2009. Intraflagellar transport particle size scales inversely with flagellar length: revisiting the balance-point length control model. *J. Cell Biol*. 187: 81-9.

18. Wren KN, Craft JM, Tritschler D, Schauer A, Patel DK, Smith EF, Porter ME, Kner P, Lechtreck KF. 2013. A differential cargo-loading model of ciliary length regulation by IFT. *Curr. Biol*. 23: 2463-71.

19. Ludington WB, Ishikawa H, Serebrenik YV, Ritter A, Hernandez-Lopez RA, Gunzenhauser J, Kannegaard E, Marshall WF. 2015. A systematic comparisoin of mathematical models for inherent measurement of ciliary length: how a cell can measure length and volume. Biophys. J. 108, 1361-79.

20. Iomini C, Babaev-Khaimov V, Sassaroli M, Piperno G. 2001. Protein particles in Chlamydomonas flagella undergo a transport cycle consisting of four phases. *J. Cell Biol.* 153: 13-24.

21. Engel BD, Ishikawa H, Wemmer KA, Geimer S, Wakabayahi K, Hirono M, Craige B, Pazour GJ, Witman GB, Kamiya R, Marshall WF. 2012. The role of intraflagellar transport in flagellar assembly, maintenance, and function. J. Cell Biol. 199, 151-67.

22. Chien, A, Shih SM, Bower R, Tritschler D, Porter ME, Yildiz A. Dynamics of the IFT Machinery at the Ciliary Tip. *eLife* 6 (September 20, 2017): e28606. https://doi.org/10.7554/eLife.28606.

23. Blasius, T. Lynne, Nathan Reed, Boris M. Slepchenko, and Kristen J. Verhey. Recycling of Kinesin-1 Motors by Diffusion after Transport. *PLOS ONE* 8, no. 9 (September 30, 2013): e76081. doi:10.1371/journal.pone.0076081.

24. Levy, E.M. (1974). Flagellar elongation as a moving boundary problem. Bull Math Biol *36*, 265-273.

25. Luo, M., Cao, M., Kan, Y., Li, G., Snell, W., and Pan, J. (2011). The phosphorylation state of an aurora-like kinase marks the length of growing flagella in Chlamydomonas. Curr Biol *21*, 586-591.

26. Cao, M., Meng, D., Wang, L., Bei, S., Snell, W.J., and Pan, J. (2013). Activation loop phosphorylation of a protein kinase is a molecular marker of organelle size that dynamically reports flagellar length. Proceedings of the National Academy of Sciences *110*, 12337-12342.

27. Hilton, L.K., Gunawardane, K., Kim, J.W., Schwarz, M.C., and Quarmby, L.M. (2013). The kinases LF4 and CNK2 control ciliary length by feedback regulation of assembly and disassembly rates. Current biology : CB *23*, 2208-2214.

Supplemental Material

Transition Matrix Model

Here we seek a more abstract model that can be analyzed mathematically to yield a more intuitive understanding of why the model works the way it does. To this end, we modeled the flagellum as a column vector N(t), with each element in the vector representing the number of motors at that location processing along the flagellum at time t. We then extended that vector to twice the length of the flagellum, with each element in the second half representing the number of motors diffusing at the corresponding location. Finally, we extended the vector by one element to represent the number of motors in the base. We can then represent the dynamics of the entire system using a stochastic matrix M such that M*N(t) = N(t+1).

Supplemental figure 1.1A shows an example transition matrix M representing the dynamics of a flagellum of length 4. To construct M, we need to consider several constraints. First, the number of motors in the system must be conserved, so the sum of the elements in the state vector N(t) must remain constant throughout all t. The columns can be thought of as the spread of a point source after one time step. Specifically, if the value of the state vector component at position j at time t is n_j , the transition matrix will redistribute those n_j motors into a new distribution, governed by the values in M. Since every motor needs to end up in some position (given conservation of total motor number), the entries in the whole column must sum to 1. The condition that each column in M must sum to 1 defines M as a left stochastic matrix. This property of the matrix will help us later determine the steady state of the system and solve the length control problem.

Second, the matrix must simulate active transport for the top half of the state vector, diffusion for the bottom half, and absorption/recruitment to send motors from the bottom value to the top value. Since we constructed the state vector such that the first L values represent bound (i.e. transporting) motors, the top left quadrant of the transition matrix M will represent the active transport dynamics. Active transport is simply moving some percent of motors one unit forward and keeping the remaining motors at their current position at each time step, so the active transport quadrant of the matrix will have positive values on the diagonal and one position under the diagonal.

The diffusion region of the transition matrix must apply to motors that have moved past position L in the state vector. This means that the lower right quadrant of the transition matrix M must simulate the dynamics of diffusion. We can incorporate the random walk nature of diffusion into this matrix by stating that the probability of staying in the same position is high, and the position of moving one position to either side is low. This simulates the Gaussian spread of a diffusing point source after a small time (we keep the time small so there is a negligible chance of diffusion two units away).

Notice that the first column incorporates the reflecting boundary condition that motors cannot go past the tip, so the odds of staying at the tip are the odds of not moving anywhere (here 0.98) plus the odds of moving past the tip and bouncing off (here 0.01). Also note that the way our state vector is constructed, motors diffusing in the direction of the base are going down the state vector towards lower rows. This matches the order in which vector elements representing diffusing kinesins are specific in the state vector.

With the aforementioned elements of M specified, we are able to represent how the motors can actively transport to the tip, unbind, diffuse back to the base, and absorb at the base so that motors enter the inactive pool. We still need to add the final element of our dynamics into the matrix: injection. A simple way to do this is to assume that at each time step, the base sends p percent of the motors in the base back to the flagellum for active transport. This means that 1-p represents the proportion of motors that stay in the base. Such an assumption is a simplified representation of the quasi-periodic avalanching process, and may need to be relaxed in future simulations. The last column in M represents the spread of motors that were previously at the base. To incorporate avalanching and recruitment into this column, we simply make the column $[p\ 0\ 0\ \ldots\ 0\ 0\ 1\text{-}p]^T$, where p is the probability of a motor being injected.

Now all the columns in the matrix sum to 1, so the condition for being a stochastic matrix are satisfied. The probability of different states evolves in a strictly deterministic manner determined by successive matrix multiplications. For example, if the diffusion half of the state vector is $[0\ 1\ 0\ 0]^T$, applying M will result in a new state vector whose elements are real numbers in the range 0 to 1 that represent the probability of a motor occupying that position in the state vector. This makes sense physically in the assumption that there are a large number of motors in the system, and since the number is on the order of 200 motors, this is a reasonable approximation.

One limitation of this construction of the transition matrix is that it assumes a constant flagellum length. The length determines the size of the matrix, so to simulate length dynamics over time, we would need to continuously alter the size of the matrix. To avoid this inconvenience, we can instead directly calculate the steady state behavior as a function of flagellar length. The steady state solution N_{ss} must satisfy $M * N_{ss} = N_{ss}$, so N_{ss} is an

eigenvector of *M* with eigenvalue 1. The Perron-Frobenius theorem states that the largest magnitude eigenvalue of stochastic, nonnegative, and irreducible matrix is always simple and equal to 1. Our motor transition matrix is stochastic (i.e. Markov) because the columns each sum to 1. It is nonnegative because all values are greater than or equal to zero. Finally, it is irreducible because each node has a path to get to every other node after some number of time steps. For example, a motor in the middle of active transport has a path leading through every subsequent active transport node, then it connects to a diffusion node, and each diffusion node is connected to a subsequent diffusion node, the last one connects to the base node, which connects to the first active transport node. This means we can apply the Perron-Frobenius theorem for nonnegative irreducible matrices to this stochastic matrix, proving that the eigenvalue of 1 always exists and is unique, and corresponds to a principal eigenvector corresponding to the steady state number distribution (N_{SS} in our example). This also means that the system is robust, and all sizes of the matrix M will yield a steady state solution. Because all other eigenvalues must have magnitudes less than 1, the corresponding eigenvectors will decay in any superposition state, so the same steady state solution will always be attained regardless of initial state. No change to the numerical values of the parameters in the model will cause the matrix M to violate the conditions of the Perron-Frobenius theorem, hence there will always be a unique steady state no matter how the parameters are altered. This property of stable length control is a robust feature of the system.

This method represents IFT in a flagellum at any fixed length, which determines the size of the state vector and transition matrix. The flagellum grows when motors with cargo reach the tip, and shrinks through a constant, length-independent decay. When the number of motors arriving at the tip times the growth per motor equals the decay in some time interval, the net

length change will be zero. Since motors in active transport move at a constant rate, the number of motors injected into active transport is the only factor that controls the number arriving at the tip per second. This value can be expressed as the number of motors in the base multiplied by *p,* the fraction of motors in the base that get injected into active transport. We can therefore define the critical rate of motors that must arrive at the tip to maintain a steady state length as $G = d/(\delta L * p)$, where d is the decay rate and δL is the growth increment when a single motor reaches the tip. The value of the steady state number density vector N_{SS} in position (2L+1) is the number of motors at the base. This means that when $N_{SS}(2L+1) > G$, there are enough motors at the tip that the flagellum will grow. If $N_{SS}(2L+1) < G$, there are too few motors to counteract the decay, so the flagellum will shrink. This means that when $N_{SS}(2L+1) = G$, the growth factor from motors at the tip perfectly cancels the decay rate. Therefore, when $N_{SS}(2L+1) = G$, the matrix is the right size to encode a flagellum that reaches steady state length.

We can find this matrix by creating transition matrices corresponding to a range of lengths, finding each matrix's principle eigenvalue, and examining the value of the corresponding eigenvector at position (2L+1). Supplemental figure 1.1B shows the values at this position as a function of L. The horizontal line represents the value of G given by the default parameters in the agent-based model. The matrix that intersects the line at G is the one with the steady state length. The difference between this steady state length and the result from the agent-based model may be explained by the different implementation of avalanching between the models. Note the inverse relationship between injection rate and flagellar length, matching experimental results (16). A possible future direction for this model is making the separation between elements in the matrix correspond to a smaller unit of length, or perhaps a continuous differential equation, allowing us to precisely predict final length. The equilibrium here is stable,

reiterating the point that the length would modulate until it reaches steady state. It also means that this system is robust, because any parameter adjustment would retain the stable equilibrium. This model also predicts that the gradient of diffusing motors is linear (Supp. fig. 1.3C), like in the agent-based model. The benefit of the matrix model in addition to the agent-based model is that it provides an intermediate level of scale that proves stability and robustness, and that it is efficient to vary biochemical parameters and find the steady state solution.

Supplemental Figures

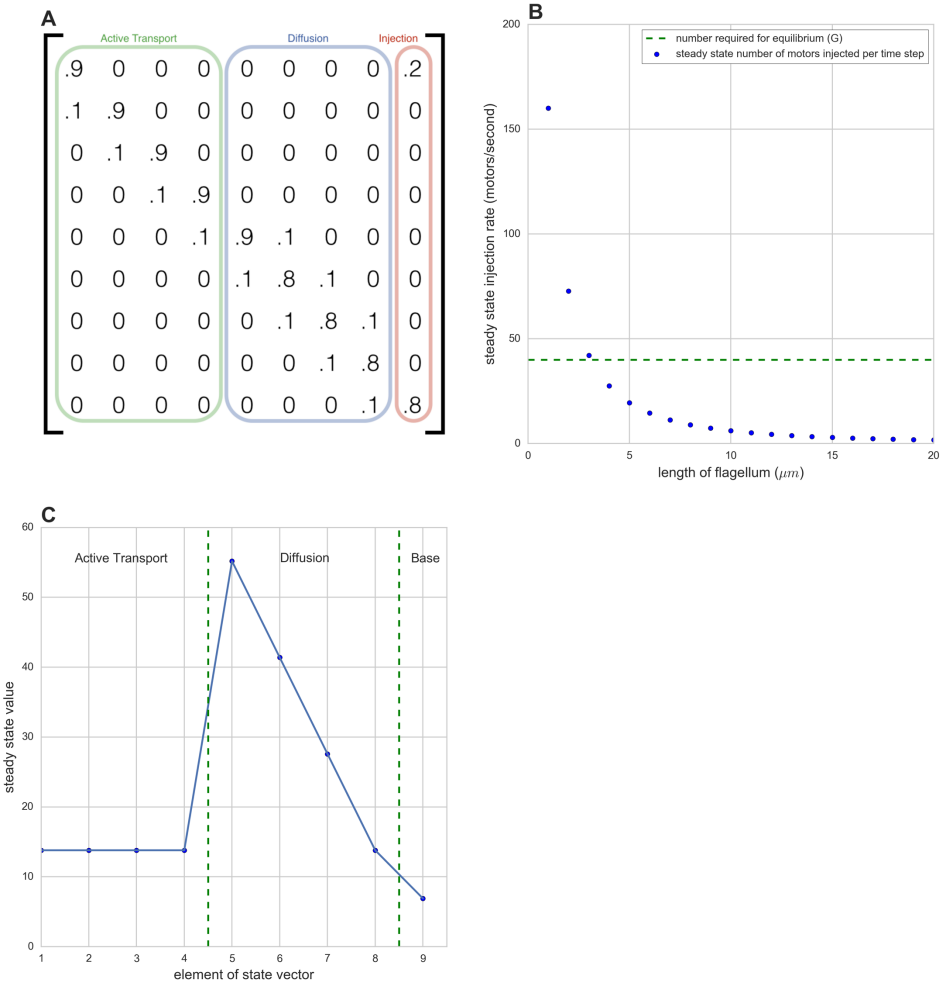

Supplemental figure 1.S1 Markov matrix model
(A) Example of a transition matrix, here with length 4, active transport rate of 0.1, diffusion spread of 0.1, and injection rate of 0.2. The relative sizes of the active transport rate and diffusion rate are roughly equal to the biological parameters used in the agent-based model, but the injection rate is simplified to a length-independent proportion. Based on the active transport and diffusion parameters, this matrix advances a state vector forward in time by 0.05 seconds. (B) Steady-state injection rate as a function of length compared to the value G required for equilibrium. (C) Steady state number density (principal eigenvector) for one set of parameters. x = 1:4 is active transport, x = 5:8 is diffusion, x = 9 is base. Note that the eigenvector can be scaled to an arbitrary magnitude, here it makes sense to normalize it to sum to the number of motors in the system, which we set to 200 for consistency with the agent-based model.

Chapter 2

Speed and Diffusion of Kinesin-2 are Competing Limiting Factors in Flagellar Length Control Model

The text of this chapter of the dissertation is a reprint of the material as it appears in Biophysical Journal. The co-authors listed in this publication directed and supervised the research that form the basis for this chapter of the dissertation. Below is a copy of the entirety of the publication:

Ma, Rui, Nathan L. Hendel, Wallace F. Marshall, and Hongmin Qin. "Speed and Diffusion of Kinesin-2 Are Competing Limiting Factors in Flagellar Length-Control Model." *Biophysical Journal* 118, no. 11 (June 2, 2020): 2790–2800. https://doi.org/10.1016/j.bpj.2020.03.034.

Abstract

Flagellar length control in *Chlamydomonas* is a tractable model system for studying the general question of organelle size regulation. We have previously proposed that diffusive return of the kinesin motor that powers intraflagellar transport can play a key role in length regulation. Here we explore how the motor speed and diffusion coefficient for the return of kinesin-2 affect flagellar growth kinetics. We find that the system can exist in two distinct regimes, one dominated by motor speed and one by diffusion coefficient. Depending on length, a flagellum can switch between these regimes. Our results indicate that mutations can affect length in distinct ways. We discuss our theory's implication for flagellar growth influenced by beating and provide possible explanations for the experimental observation that a beating flagellum is usually longer than its immotile mutant. These results demonstrate how our simple model can suggest explanations for mutant phenotypes.

Statement of Significance

The eukaryotic flagellum is an ideal case study in organelle size control because of its simple linear shape and well-understood building mechanism. In our previous work, we proved that flagellar length in the green algae *Chlamydomonas* can be controlled by the diffusive gradient of the kinesin-2 motors that deliver building blocks to the tip. In this study, we expand on the analytical formulation of the diffusion model to show how physical parameters affect final length and regeneration time, enhancing the model's potential to explain length mutants and motivate future research with precise predictions.

1. Introduction

Biologists have long been trying to understand how cells build themselves. The proteins that cells synthesize must come together to form massive organized structures without any guidance. A striking case of this is that some single-celled organisms can regenerate missing pieces, implying that the cell has some form of design specifications embedded within it that allow the cell to reconstruct the correct form. The single-celled algae *Chlamydomonas reinhardtii* is an ideal organism for studying single cell organelle regeneration because it has two linear flagella that grow back upon being cut or shed (1). The kinetics of flagellar growth have been well documented, and much is known about the inner components of the flagellum and its growing process, but how the flagellum consistently reaches the same steady-state length is a mystery. Multiple different theoretical models have been developed to explain this robust regeneration, and recent work demonstrated the feasibility of a model in which the length of the flagellum is governed by a diffusive gradient across its length (2, 3).

In this study, we further develop the diffusion model by deriving the growth curve analytically as a function of time and the relevant physical parameters. This shines light onto which factors are limiting at different stages in the growth. It also lets us predict steady-state length from observed physical parameters and predict physical parameters from observed steady-state length.

In order to understand the length control model, one must first understand how a *Chlamydomonas* cell builds its flagella. The flagellum is made of nine doublet microtubules, and to get longer, new tubulin (the building blocks of microtubules) must be delivered to the flagellar tip. The mechanism for transporting tubulin to the tip is called intraflagellar transport, or IFT (4–8). In IFT, tubulin and other building materials such as axonemal dynein arms are bound to

protein complexes of ~20 polypeptides called IFT particles. These IFT protein complexes form linear arrays called "trains" and are pulled to the distal tip by heterotrimeric kinesin-2 motors (9–12). Upon arrival at the tip, the tubulin and other building blocks are added to the flagellum, increasing its length. To counter this length increase, tubulin is continually removed from the flagellar tip at a constant, length-independent rate (13, 14). Cytoplasmic dynein-2 motors carry the IFT particles back to the base (15, 16). IFT happens continuously throughout the lifespan of a *Chlamydomonas* cell, and when the rate of IFT-driven assembly equals the rate of length-independent tubulin removal, steady-state length is achieved.

IFT begins through a process called "injection" in which IFT trains are released from docking sites at the flagellar basal body and transition zone and transported into the flagellum itself (17). Injection is not fully understood, but it appears that IFT material injects into the flagellum from the basal body upon accumulation of motors in the basal body. Quantitative live cell imaging has shown that the rate of injection is a decreasing function of the length of the flagellum (18, 19). This implies some sort of sensing mechanism that allows the basal body to sense the flagellar length. The sensing mechanism here is unknown, and is the core puzzle that length control models try to solve (18, 20, 21).

The flagellar length regulation problem is an ideal system for mathematical biology because the flagellum has a simple geometry, easily simplified building and degrading process, and a mysterious control mechanism that has eluded scientists of all disciplines for generations. As a result, there have been several models for length control that have been studied in detail (20). Some models, such as the time-of-flight model in which the IFT particles can be somehow deactivated if they have been in the flagellum for a long time, have been ruled out when experiment failed to confirm predictions from the model (21). Several models can still explain all

experimental results, including the ciliary current model in which ion channels lining the flagellum at regular intervals regulate the electric potential inside the flagellum and thus regulate length (20). In this study we will further develop the diffusion model, in which the length-dependent rate of IFT is generated by the kinesin motors diffusing back to the basal body from the tip, using the time it takes to diffuse back as a proxy for length measurement (2). One reason that we focus on this model is that the diffusion model is the most parsimonious in the sense that it does not require any additional components other than those already known to explain length regulation. The other models require additional molecular components to transduce a length-dependent signal to the IFT injection system. Moreover, the diffusion model has the most support from experimental results, most notably from a recent study in which kinesin motors were observed to diffuse from the tip to the base but are not actively transported back to the base (22), while the other components of IFT trains are transported back to the flagellar base by IFT dyneins (15, 16). When retrograde IFT stopped, all other parts of the IFT train, but not kinesin, are accumulated at the flagellar tip (23). By further developing the diffusion model, we make predictions that will motivate experiments that would not have been obviously useful in distinguishing length control models.

In the model explored by Hendel et al., the longer the flagellum, the longer it takes for kinesins to diffuse back to the base, and therefore the longer it takes for enough kinesins to accumulate in the base to power injection (2). This explains, in principle, how longer flagella inject less building material per second. The model assumes that kinesins are conserved and not drawn from the cell body in significant number. This would eliminate the need for a currently undiscovered signaling pathway, and would allow the already-known components of IFT to generate its own length dependence. In this study, we will take the conclusions from Hendel et

al. and further develop the analytical formalism of the diffusion model to show how altering the diffusion coefficient and IFT velocity would affect observables like steady-state length and regeneration time (2). Hendel et al. mainly focused on diffusion coefficient and briefly focused on motor velocity, but here we examine flagellar growth when considering these two parameters together. This study provides a mean-field description of our previous stochastic simulations in Hendel et al., 2018. The model is mathematically rigorous and analytically tractable, thus providing a clearer picture to look at different regimes for different parameters than the stochastic simulations. We identified three factors that limit flagellar growth at different phases of its regeneration, which lead to two possible rate-limiting steps of flagellar growth at steady state. We then used the upgraded model to attempt to explain observed length changes in length-altering mutants by calculating what changes in diffusion coefficient and IFT velocity are necessary. We arrived at the conclusion that changes in diffusion coefficient may be responsible for the length changes in the mutants.

2. Model

We treat the flagellum as a linear track for kinesin motors (Figure 2.1). The position on the track is labeled by x with $x = 0$ corresponding to the base and $x = L(t)$ corresponding to the tip of the flagellum, where $L(t)$ is the length of the flagellum at time t. We distinguish four populations of kinesin motors: (i) motors that actively carry cargos from the base to the tip with a constant velocity v; (ii) motors that accumulate at the tip after the delivery; (iii) motors that diffuse back to the base from the tip with a diffusion coefficient D; (iv) motors that accumulate at the base when diffusion is completed.

The linear number density of active motors $\rho_a(x,t)$ of type (i) is governed by the equation

(2.1a) $\partial_t \rho_a(x,t) = -\partial_x J_a(x,t)$,

with the convective current

(2.1b) $J_a(x,t) = v\,\rho_a(x,t)$.

The number of type (ii) motors N_t dwelling at the tip is described by

(2.2) $\frac{dN_t}{dt} = J_a(L,t) - k_t N_t$,

where k_t is transition rate for a motor dwelling at the tip switching to a diffusive state.

The linear number density of diffusive motors $\rho_d(x,t)$ of type (iii) obeys the simple diffusion law:

(2.3a) $\partial_t \rho_d(x,t) = -\partial_x J_d(x,t)$,

with the diffusive current

(2.3b) $J_d = -D\partial_x \rho_d(x,t)$.

The number of type (iv) motors N_b accumulating at the base is described by

(2.4) $\frac{dN_b}{dt} = J_d(0,t) - k_i N_b$,

where k_i is the injection rate of motors from the reservoir at the base to the flagellum track. Experimental evidence indicates that injection actually resembles a threshold switch (18), but since this version of the model is a mean field description rather than a stochastic simulation, we decided to approximate the thresholding as a first-order process in which injection is proportional to the number of motors in the base. On average, this will result in the same number of injections per second. This is especially true in steady state, when the rate of injection is also at steady state.

The total number of motors N includes all four populations of motors and reads

(2.5) $N = N_b + N_t + \int_0^L (\rho_a + \rho_d)dx$.

We assume the total number of motors is conserved and this imposes the boundary conditions at the base

(2.6a) $J_a(0,t) = k_i N_b$,

and at the tip

(2.6b) $J_d(L,t) = k_t N_t$.

The growth dynamics of the flagellum are governed by the equation

(2.7) $\frac{dL}{dt} = J_a(L,t)\delta - r_d$,

where δ denotes the length elongation caused by the arrival of a single kinesin motor, and r_d denotes the de-polymerization speed which is independent of the length.

3. Results

We can numerically solve the dynamic equations of (2.1)-(2.4) and (2.7) to have the exact growth curve $L(t)$ for a flagellum of length L as a function of time t. The parameters used in our numerical solutions are listed in Table 1. Due to the small elongation increment δ, we can also make a quasi-static assumption that at each length L, the spatial distribution of molecular motors reaches steady state for that particular length L (see Appendix A). The analytical results obtained by this quasi-static assumption almost exactly overlap with the exact numerical solution (Figure 2.2a, c and e). Therefore, for the rest of the paper we only show results obtained with the quasi-static assumption.

3.1. The rate-limiting step changes as the flagellum grows

Typical growth curves of the flagellum are demonstrated in Figure 2.2 for three diffusion coefficients. Each growth curve rapidly increases at first and then slowly plateaus to the steady-state length. The growth can be divided into different stages based on the rate-limiting step. To see this, we express the growth rate of the flagellum under the quasi-static assumption as

(2.8) $\frac{dL}{dt} = \frac{N\delta}{\frac{L}{v} + \frac{L^2}{2D} + \frac{1}{k_t} + \frac{1}{k_i}} - r_d = \frac{N\delta}{t_{\text{active}} + t_{\text{diff}} + t_{\text{dwell}}} - r_d$,

where $t_{\text{active}} = \frac{L}{v}$ denotes the time for a motor to transport the assembly unit of the flagellum from the base to the tip, $t_{\text{diff}} = \frac{L^2}{2D}$ denotes the root-mean-square time for a motor to diffuse back to the base from the tip, and $t_{\text{dwell}} = \frac{1}{k_t} + \frac{1}{k_i}$ denotes the total time a motor dwells at the base and at the tip. At short length scale, t_{dwell} always dominates over the other two time scales, and motors spend most of their time dwelling at the tip and the base (Figure 2.2b, d and f, green lines). In this regime, the duration that the motor spends traveling between the base and the tip is negligible, so the flagellar growth rate is independent of length. When the flagellum grows longer, either the diffusive time t_{diff} dominates if D is small (Figure 2.2b), or the transportation time t_{active} dominates if D is large (Figure 2.2f). For an intermediate D, the growth is divided into three stages, in which the dominant time scales are t_{dwell}, t_{active} and t_{diff} (Figure 2.2d). Measurements of flagellar growth kinetics have clearly shown that growth rates are constant for flagella shorter than 4-5 microns (1). In a different algal species, Spermatozopsis similis, flagella grow at a constant rate over their whole length, suggesting that in that organism, t_{dwell} is always the dominating factor (20).

3.2. Diffusion vs. active transport as the rate-limiting step at steady state

The diffusion time t_{diff} scales with L^2, while the motor transportation time t_{active} scales with L. At steady state, depending on the flagellar length L^{ss}, either active transport or motor diffusion becomes the rate-limiting step. For a sufficiently long flagellum, t_{diff} always dominates over t_{active}. However, the steady-state length L^{ss} might not be long enough to have t_{diff} greater than t_{active}. In Figure 2.3a, we show the three time scales at steady state as a function of diffusion coefficient D. For small D, t_{diff} dominates over the other time scales. However, as D increases, t_{active} becomes greater than t_{diff}, and the steady-state length of the flagellum becomes limited by the active motor transport. If we fix the diffusion coefficient but vary the motor velocity, the growth will change from t_{active}-dominance to t_{diff}-dominance (Figure 3B). A phase diagram is shown in Figure 2.3c. Generally, a larger diffusion coefficient D favors motor-limited growth, and a faster motor speed v favors diffusion-limited growth.

3.3. A dramatic increase in steady-state length L^{ss} requires a dramatic increase in diffusion coefficient D if motor velocity v is small

The steady-state length of the flagellum L^{ss} can be obtained by setting $\frac{dL}{dt}$ in Equation (2.8) to zero. This leads to the analytical result

$$(2.9)\ L^{ss} = -\frac{D}{v} + \sqrt{-\frac{2D}{k_i} - \frac{2D}{k_t} + \left(\frac{D}{v}\right)^2 + \frac{2DN\delta}{r_d}}.$$

The steady-state length L^{ss} increases with both diffusion coefficient D and motor velocity v. For a small motor velocity, increasing the diffusion coefficient does not lead to significant increase in L^{ss} because it is mainly set by the small motor velocity (Figure 2.4a, green line). For instance,

if the motor velocity v is $1\mu m/\mathrm{s}$ and L^{ss} is $5\mu m$, it would be impossible to increase the length to 10 μm because even in the limit of an infinitely large diffusion coefficient $D \to \infty$, the maximum length L^{ss} is $9.5\mu m$. The analytical proof of this limit is derived in Appendix B.

However, if the motor velocity v is 2 $\mu\mathrm{m/s}$, the diffusion coefficient D must only increase from 1.8 $\mu\mathrm{m}^2/\mathrm{s}$ to 11.1 $\mu\mathrm{m}^2/\mathrm{s}$ to increase the length to ten microns, the typical length of wild type *C. reinhardtii* cells. Similarly, for a small diffusion coefficient, increasing the motor velocity does not lead to a significant increase in L^{ss} either (Figure 2.4b, green line).

3.4. Growing time T of the flagellum increases with motor velocity and diffusion.

In this section, we study the time T a flagellum needs to grow to its steady state. We define the growing time T as the amount of time to reach 95% of the steady-state length, i.e., $L(T) = 0.95\ L^{ss}$. Figure 2.5 plots numerical solutions of T as a function of motor speed and diffusion coefficient. One might expect that a fast-transporting motor or a fast-diffusive motor will reduce the time to construct a flagellum, but the results show that the growing time T increases with the diffusion coefficient D and the motor velocity v (Figure 2.5a and b). This is because the steady-state length also increases with D and v. The reduction in time due to increased v or D cannot compensate for the increased time due to length elongation.

3.5. Parameter changes that maintain the steady-state length but alter the growing time.

One may notice that the contour lines for the steady-state length L^{ss} do not exactly overlap with the contour lines for the growing time T (Figure 2.6a). The implication of this difference is that growth kinetics do not uniquely determine the steady-state length, and one can alter the growing time T while maintaining the steady-state length L^{ss} constant, or vice versa. A

recent experiment found that mutants in ida5, which affect actin, show slower growth kinetics (i.e. longer T) but reach the same steady-state length as wild-type (24). Based on our model, this could be a result of the combination of reduced motor velocity and enhanced diffusion coefficient (Figure 2.6b and c). Our model predicts that the change in the growing time is larger for longer flagella, which can be tested by future experiments.

4. Discussion

In this paper, we have presented a mean field description of our previous stochastic simulation to account for flagellar growth. The key to achieving length regulation is that the number of kinesin motors is finite. As the flagellum elongates, it takes more time to transport the assembly unit from the base to the tip and to retrieve the kinesin motors from the tip to the base, therefore the assembly rate of the flagellum is reduced. Steady-state length is reached once the assembly rate equals the disassembly rate. This reaction-diffusion based mechanism of length regulation is also present in the growth of stereocilia, which are made of a bundle of actin filaments (25), and a series of models have indeed shown that the reaction-diffusion mechanism is sufficient to account for length regulation in that organelle (25-27). We have modeled a reaction-diffusion mechanism for flagella which, because it also involves an interplay between motors and diffusion, ends up being quite similar in its form to the previously described models for length regulation in stereocilia. However, in stereocilia, the polymerization rate of actin filaments is reduced by the resisting force from the membrane. The steady-state length is reached when the retrograde flow of actin filaments is balanced by actin polymerization at the tip (25–27). We also note that in the present version of our model, we only consider the growth of a single flagellum but neglect the coupling between the two flagella for *Chlamydomonas*. In ref. (28), the authors studied the coupling mechanism to account for length equalization when one of

the flagella is severed. In our model, length equalization can be achieved by having a shared pool of tubulins and replenishment of kinesin motors (2).

A large part of the explanatory and predictive power of the model is in generating hypotheses to explain length mutants and motivating experiments to test these hypotheses. We can now examine a length mutant, note its length change from wild type, and determine what changes in velocity and diffusion are necessary to achieve the length change. Here we discuss *pf14*, a mutant that is missing the radial spoke head in the flagellum. In wild-type *Chlamydomonas*, the two flagella beat in a cyclic pattern resembling a breast stroke: a semi-circular power stroke to swim forward followed by a recovery stroke to return them to their initial position. *pf14*, on the other hand, has paralyzed flagella and cannot swim. What is puzzling about this mutant is that its flagella are about half as long as wild type. *pf14* mutants are 3-6 μm in length, while wild type flagella are usually 10-12 μm (29). This short flagella phenotype is common among the group of motility mutants, especially the ones with completely paralyzed flagella (30–35). To our knowledge, no study has explained the connection between paralysis and length decrease – in fact, researchers have viewed intraflagellar transport and flagellar beating as two independent processes. This is reasonable, since beating relies on axonemal dynein and other regulatory and structural components to bend doublet microtubules, components that are not involved in IFT. Even when detached from the cell body, the flagellum equipped with the motility apparatus is capable of producing a high-frequency waveform as long as ATP is provided (36).

While it is possible that the length change comes from a structural instability caused by the mutation, could it instead be because the paralysis of the flagella alters the IFT-diffusion system that could be responsible for length control? All existing measurements of IFT kinetics

have been carried out in immotile flagella, either in paralyzed mutants or in wild-type cells whose flagella are adhered to a glass surface. Consequently, there is no experimental information about how IFT kinetics might or might not change in beating flagella compared to immotile flagella. Here we use our model to explore the plausibility of the idea that flagellar beating can influence IFT kinetics and thus might act as a wrongfully neglected factor in the length control system. In the sections below, we propose mechanisms through which flagellar beating can influence IFT kinetics. Through some back-of-the-envelope calculation, we show the effective contribution of each mechanism to the length change of motile flagella compared with immotile ones. We focus on mechanical mechanisms that are directly related to flagellar beating, but neglect chemical mechanisms that might exist in the mutants. For instance, experiments have shown that the presence of substrate can enhance the diffusion of substrate (37, 38). The diffusion constant of kinesin motors therefore can be influenced by ATP concentration in wild type and in mutants. This biochemical regulation is out of the realm of the paper.

4.1. An increase in diffusion coefficient is necessary for the increase of steady-state length.

Based on our model, there are four aspects of IFT kinetics that can be influenced by flagellar beating. They include kinesin motors dwelling at the base and at the tip, actively transporting from the base to the tip, and passively diffusing from the tip to the base. Altering the dwelling time of kinesin motors at the tip or at the base has a minor effect on the steady-state length of flagella. This is because the rate-limiting step at steady state is either active transport or passive diffusion, as have demonstrated in section 3.2. With the parameters given in Table 1 but a low diffusion constant $D = 2\ \mu m^2/s$ for an immotile flagellum, even if the injection rate increases from 1 s^{-1} to infinity, the steady-state length only increases from 5.2μm to 5.5μm

according to Eq. (2.9). Therefore, we exclude the possibility of an altered injection rate at the base or an altered dwelling time at the tip as the explanation for the length difference between motile and immotile flagella. We consider the other two aspects of IFT kinetics for the significant increase in length in a beating flagellum compared to an immotile one: (i) The motor velocity remains unchanged and the increase is due to enhanced diffusion. (ii) The diffusion coefficient remains unchanged and the increase is due to increased motor velocity. In a paralyzed mutant, the experimentally measured diffusion coefficient is $D = 1.68 \pm 0.04\ \mu m^2/s$ and the motor velocity is $v = 2.1 \pm 0.4\ \mu m/s$ (22). With assumption (i), to account for length increase in a beating flagellum from $5\mu m$ to $10\mu m$, the diffusion coefficient needs to increase from $1.75\mu m^2/s$ to $10.55\ \mu m^2/s$. With assumption (ii), it is impossible to account for the length increase because even in the limit of infinitely large motor velocity $v \to \infty$, the length of the flagellum approaches a maximum of $5.65\mu m$. Therefore, an enhanced diffusion coefficient is necessary and sufficient to account for the observed length increase. In any case, there is no plausible way that flagellar beating would alter the velocity of the motor. However, we can imagine several ways that beating could alter the diffusion coefficient of kinesin, which we will consider in turn.

4.2. Centrifugation effect of kinesin motors

The first mechanism we considered was inspired by the experimental observation that kinesin-2 is less dense than the flagellar matrix and floats to the top when a matrix preparation is centrifuged at high speed (H. Qin unpublished data). Based on this observation, we consider a model in which the roughly circular beating of the flagellum is enough to cause a significant centripetal force on the kinesin motors back towards the base, speeding up the diffusive return time. To model this scenario, we approximated the flagellum and its beating as a cylindrical rod

revolving around one of its ends like the hand of a clock. The contents of the cylinder will experience a centrifugation effect, and the kinesins will move towards the base if they are less dense than the surrounding solution. While this is not equivalent to increasing the diffusion coefficient, it is an increase in the speed of diffusive return. Approximating the beating as a circular motion will exaggerate the centripetal force because the recovery stroke of the beating does not have the same circular appearance as the power stroke. To estimate the magnitude of this effect, we solved the equation for centripetal force to obtain the drift velocity:

(2.10) $v_{\text{drift}} = \frac{(m-m_0)\omega^2 r}{\xi}$,

where m is the mass of kinesin, m_0 is the mass of the solution displaced by the motor, ξ is the friction coefficient (equal to kT/D where k is Boltzmann's constant, T is the temperature, and D is the diffusion coefficient), ω is the rotation rate, and r is the length of the rod. Plugging in the relevant values $D = 2\ \mu\text{m}^2/\text{s},\ kT = 4.1\ \text{pN}\cdot\text{nm},\ m = 0$ (extreme case where kinesins are massless, to give the maximum possible effect), $m_0 = 4 \times 10^{-22}$ kg, $\omega = 300\ \text{rad/s}$, and $r = 10\mu\text{m}$, we get that the drift velocity v_{drift} is on the order of $10^{-7}\ \mu\text{m/s}$, which means it would take three years for the kinesins to get from the tip to the base with this effect alone. If we translate the time sped up by the centrifugation drift into diffusive time, it amounts to an effective diffusion constant of D_{eff} which satisfies

(11) $\frac{r^2}{2D_{\text{eff}}} = \frac{r}{v_{\text{drift}}}$.

The effective diffusion constant increase D_{eff} is only on the order of $10^{-6}\ \mu\text{m}^2/\text{s}$, which is negligible compared with measured value of $D \sim 2\mu\text{m}^2/\text{s}$. We can therefore rule out the centrifugation effect as a means of generating any substantial length increase upon beating.

4.3. The increased diffusion coefficient in a beating flagellum might be explained by shear-thinning.

An alternative way that flagellar beating could influence diffusive return of kinesin is via shear of the flagellar matrix (Figure 2.7a). If we think of the flagellum as an elastic rod, when it is bent, parts of the rod are stretched and parts are compressed. The maximum shear displacement Δ can be calculated as (39).

(10) $\Delta = a[\psi(s,t) - \psi(0,t)]$,

where a is the radius of the rod, and $\psi(s,t)$ is the tangent angle along the arclength s at time t. The corresponding shear rate is

(11) $\chi = \frac{1}{a}\frac{d\Delta}{dt}$.

We select 7 frames in a periodic beating cycle of a flagellum and calculate the shear displacement and shear rate by measuring the tangent angle at equally spaced points along the arclength of the flagellum (Figure 2.7 b-f). In a beating period of $T = 0.014\ s$ (40), the variation of the shear displacement $\delta\Delta \equiv \max(\Delta) - \min(\Delta)$ is typically around 0.4 μm. Here the maximum and minimum are taken with respect to the time t in a period. The shear displacement of the flagellum can induce shear flow in the cytoplasm and this shear flow can enhance the diffusion of particles in the cytoplasm. To estimate how this affects the diffusion coefficient, we adopted Taylor dispersion theory which yields an estimate of the diffusion coefficient amplified by the shear flow by a factor of $1+Pe^2/192$, where $Pe = d\ v_{\text{shear}}/D_0$ is the Péclet number, with $d \sim 0.25$ μm being the diameter of the flagellar cross-section, $v_{\text{shear}} = \frac{\delta\Delta}{T} \sim 28$ μm/s being the shear flow rate, and $D \sim 2\ \mu m^2/s$ being the diffusion constant without shear flow (41). These

numbers give a Péclet number $Pe \sim 3.5$, and the resulting amplification factor 1.06 is too small to account for the required increase in diffusion constant. We thus conclude that shear is not large enough to increase diffusion constant significantly by means of an advective mechanism. Could shear have any other effect?

It is well known that solutions made of soft polymers become less viscous under shear deformation. This effect is known as shear thinning. In an equilibrium solution, the diffusion coefficient D of a particle and its friction coefficient ξ obey the Einstein relation $\xi D = k_B T$, where k_B is the Boltzmann constant, and T is the absolute temperature. Because the friction coefficient ξ is proportional to the viscosity η, we would expect that the product of the viscosity η and the diffusion coefficient D is also a constant. Therefore, a reduction in viscosity η caused by shear-thinning might account for the increase in diffusion coefficient D. Based on our measurements, the maximum shear rate $|\chi|_{max} \equiv \max(|\chi|)$ of the flagellum is around $600\ \mathrm{s}^{-1}$ (Figure 2.7F). The onset shear thinning rate for biopolymer solutions depends on many factors, such as protein concentration, temperature, ionic strength and even the geometry of the container. The typical onset shear thinning rate for a polysaccharide solution is $\sim 10\ s^{-1}$ and the reduction in the viscosity can be orders of magnitude (42). Recent work on bioink (alginate plus cellulose) shows that the shear thinning effect takes place at very low shear rate (43). Therefore the shear magnitude is large enough to potentially cause shear thinning in the matrix of flagella, and this effect may contribute to enhanced diffusion by reducing the viscosity. Our results thus suggest a novel hypothesis to explain the link between flagellar motility and length, namely, that paralyzed mutants have shorter length because the diffusion constant for kinesin is decreased due to a loss of shear thinning in the flagellar matrix. Our modeling results suggest a need for future experiments to measure viscosity inside the matrix.

Appendix

A. Derivation of the growth rate (8) under quasi-static assumptions.

In physiological conditions, the length elongation of flagellum is much slower than the motor transportation-diffusion cycle. This is reflected in the small elongation unit δ in Eq.(2.7). We can therefore make the quasi-static assumption that at any fixed length L, the distributions of the four populations of motors reach steady state for that particular L. This implies that all the time derivatives in Eqs. (1-4) become zero. The distribution of the active motors (i) is homogenous over the flagellum track, and the constant density reads

(2.A1) $\rho_a^s = \rho_a^0 = \frac{N/v}{\frac{L}{v}+\frac{1}{k_t}+\frac{1}{k_i}+\frac{L^2}{2D}}$

For the diffusive motor, the spatial distribution shows a gradient and reads

(2.A2) $\rho_d^s = \rho_d^0 \frac{x}{L} = \frac{N(L/D)}{\frac{L}{v}+\frac{1}{k_t}+\frac{1}{k_i}+\frac{L^2}{2D}} \frac{x}{L}$.

For the motors accumulated at the base, the number is

(2.A3) $N_b = \frac{N/k_i}{\frac{L}{v}+\frac{1}{k_t}+\frac{1}{k_i}+\frac{L^2}{2D}}$.

For the motors accumulated at the tip, the number is

(2.A4) $N_t = \frac{N/k_t}{\frac{L}{v}+\frac{1}{k_t}+\frac{1}{k_i}+\frac{L^2}{2D}}$

Substituting Equation (2.A1) into (2.7), we obtain (2.8), which is the key equation of our discussion for the dynamics of flagellum growth.

B. Derivation of the steady-state length in the limit of large diffusion coefficient

Denoting $\beta = -\frac{1}{k_i} - \frac{1}{k_t} + \frac{N\delta}{r_d}$, we can rewrite Eq. (2.9) as

(2.B1) $L^{ss} = -\frac{D}{v} + \sqrt{\left(\frac{D}{v}\right)^2 + 2\beta D} = -\frac{D}{v} + \frac{D}{v}\sqrt{1 + \frac{2\beta v^2}{D}}$.

In the limit of $D \to \infty$, we can invoke the Taylor series $(1+x)^k = 1 + kx + O(x^2)$ for $|x| \ll 1$ to expand the term in the square root and get

(2.B2) $L^{ss} = -\frac{D}{v} + \frac{D}{v}\left(1 + \frac{1}{2} * \frac{2v^2\beta}{D} + O\left(\frac{1}{D^2}\right)\right) = v\beta + O(\frac{1}{D})$.

Therefore $L^{ss} \to v\beta$ in the limit of $D \to \infty$.

The expression of $v\beta$ can be also derived in an intuitive way: at steady state the total length $N\delta$ delivered by kinesin motors divided by the time for such delivery $\frac{L^{ss}}{v} + \frac{1}{k_t} + \frac{1}{k_i}$ must equal to the depolymerization rate r_d.

(2.B3) $\frac{N\delta}{\frac{L^{ss}}{v} + \frac{1}{k_t} + \frac{1}{k_i}} = r_d$

Solving Eq. (2.B3) gives exactly $L^{ss} = v\beta$.

Table 2.1: Parameters of the model.

Parameters	Description	Reference Value	Varied range	References
v	Kinesin motor velocity	2 μm/s	0.1 – 10 μm/s	(22)
D	Kinesin motor diffusion coefficient	20 $\mu m^2/s$	0.1 – 80 $\mu m^2/s$	(22)
k_i	Injection rate of motors at the base	1 s^{-1}	1 s^{-1}	Arbitrary
k_t	Transition rate to diffusive state for motors dwelling at the tip	0.5 s^{-1}	0.5 s^{-1}	(22)
r_d	Spontaneous depolymerization speed of flagellum	0.004 μm/s	0.004 μm/s	(24, 44)
N	Total number of motors	40	40	(13)
δ	Elongation length of the flagellum upon the arrival of a motor at the tip	0.00125 μm	0.00125 μm	(13)

Figures

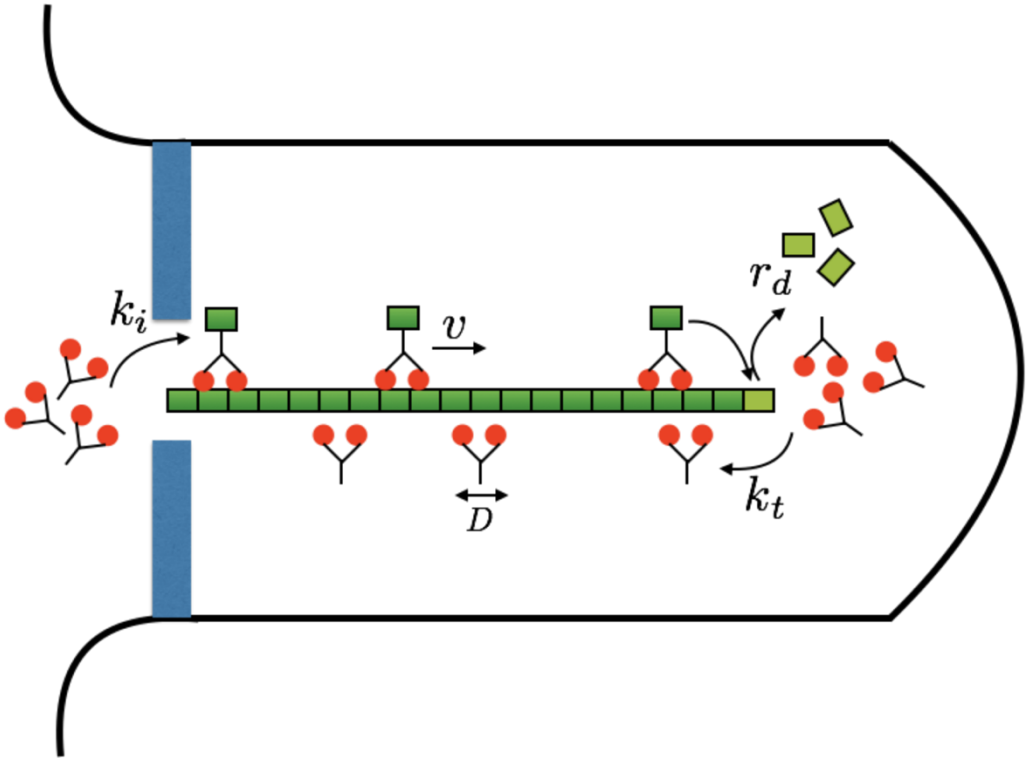

Figure 2.1: Illustration of the model
Molecular motors carry the building blocks for flagellar assembly from the base to the tip and travel with a constant speed v. When reaching the tip, the motors unload the cargo and the flagellum elongates by a unit of δ. The motors dwell at the tip and switch to a diffusive state with a transition rate k_t. The motors diffuse back to the base with a diffusion coefficient D and accumulate at the base, waiting for injection into the flagellum with a transition rate k_i. The flagellum has a spontaneous disassembly rate of r_d. The total number of molecular motors is assumed to be constant.

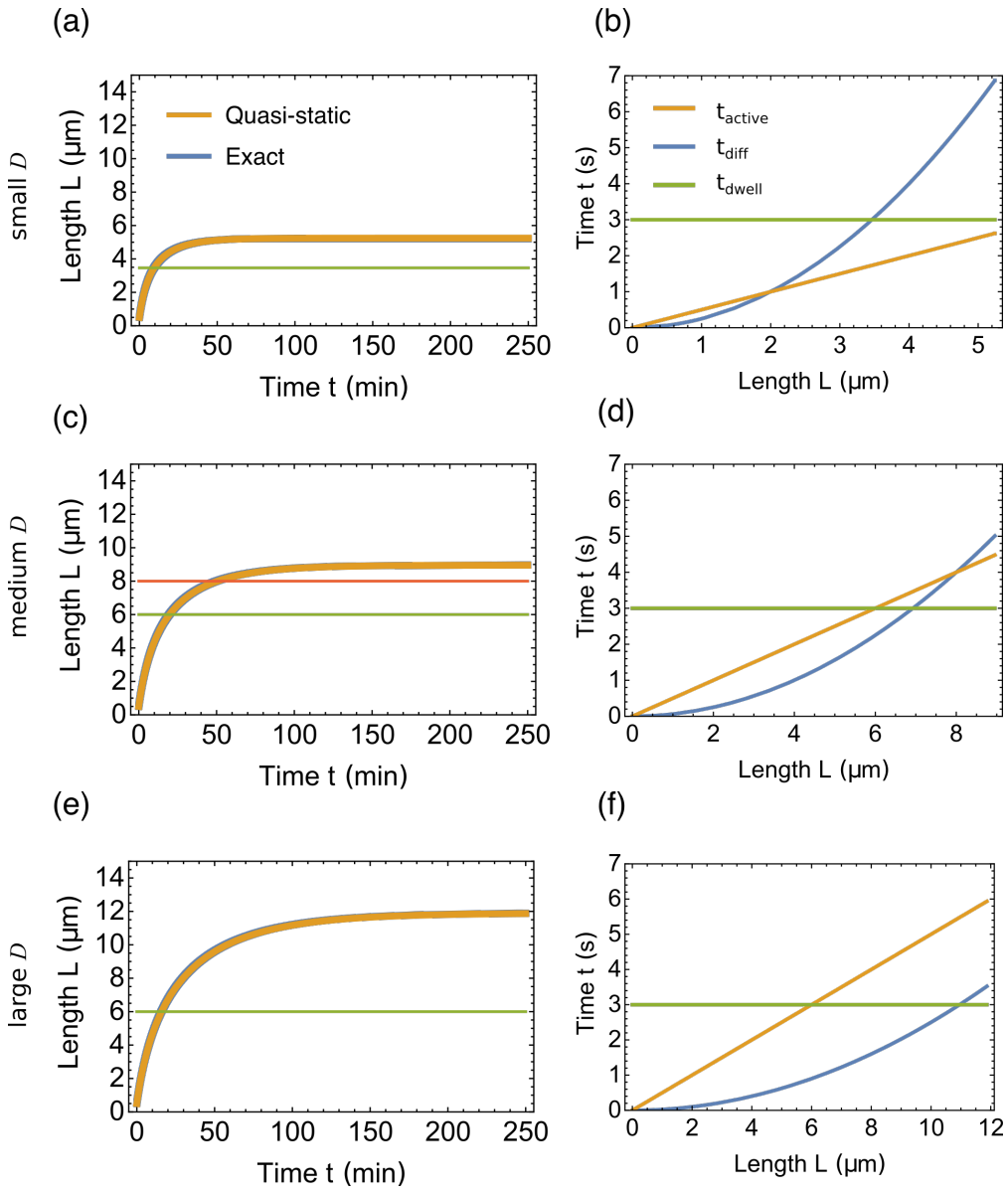

Figure 2.2: Growth dynamics of the model
(a, c, e) Growth curve of the flagellum for small diffusion coefficient $D = 2\ \mu m^2/s$ in (a), medium $D = 8\ \mu m^2/s$ in (c) and large $D = 20\ \mu m^2/s$ in (e). The blue curve represents the numerical solution, i.e., the exact solution. The orange curve represents the analytical solution obtained by the quasi-static assumption. The two curves almost overlap to the extent that the blue one is invisible. The horizontal lines represent the length at which the rate limiting step changes. (b, d, f) The time a single motor spends on different steps during a transportation-diffusion cycle for the same diffusion coefficient as in (a, c, e). The three curves include t_{active} for a motor to travel from the base to tip (orange), t_{diff} for a motor to travel from the tip to the base via diffusion (blue), and t_{dwell} for a motor to dwell at the tip waiting before diffusing and at the base waiting for injection (green).

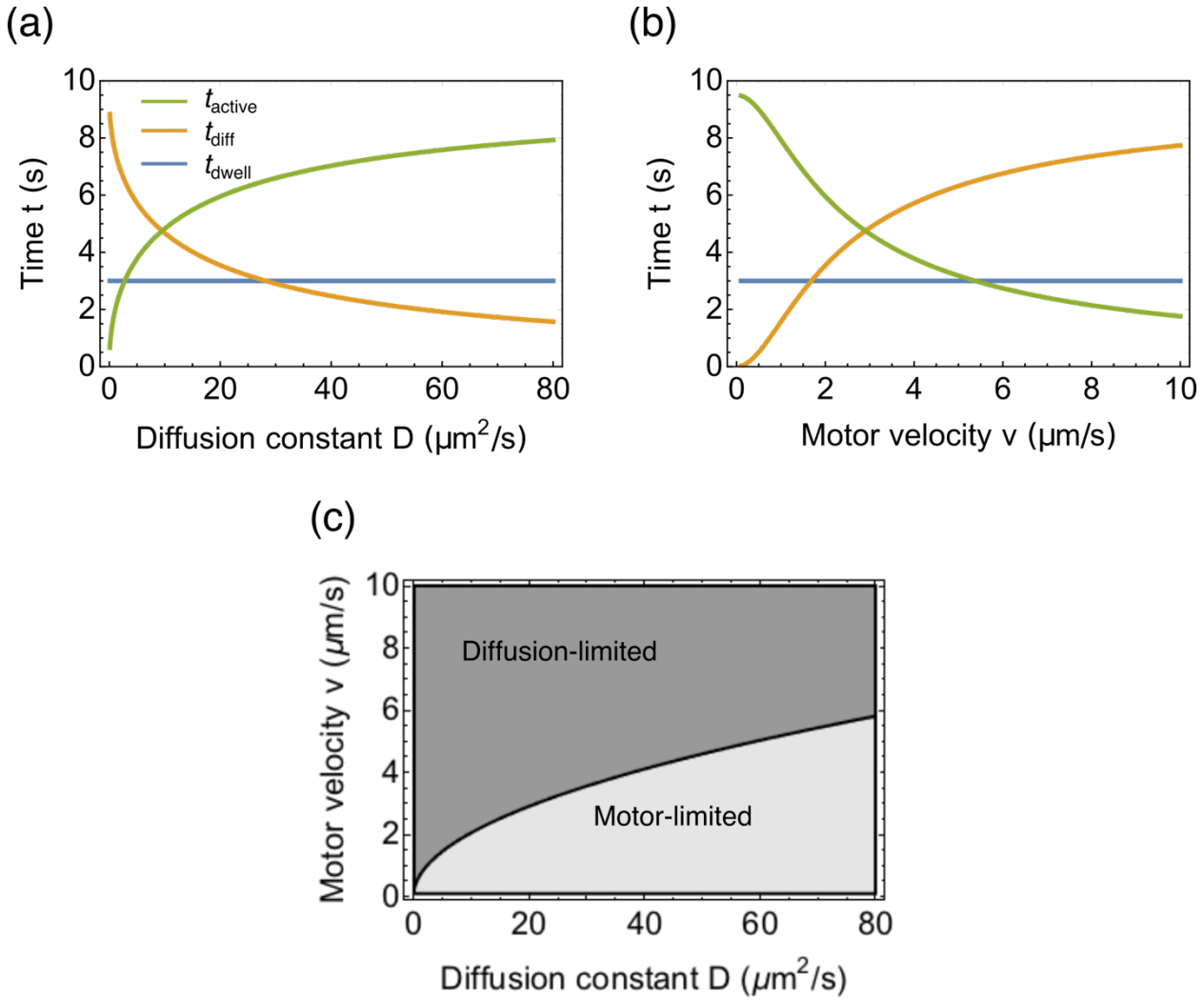

Figure 2.3: Influence of the motor velocity v and diffusion coefficient D on the rate-limiting step at steady state
(a) The three time scales as a function of diffusion coefficient D. (b) The three time scales as a function of motor velocity v. (c) Phase diagram for the rate limiting step at steady state.

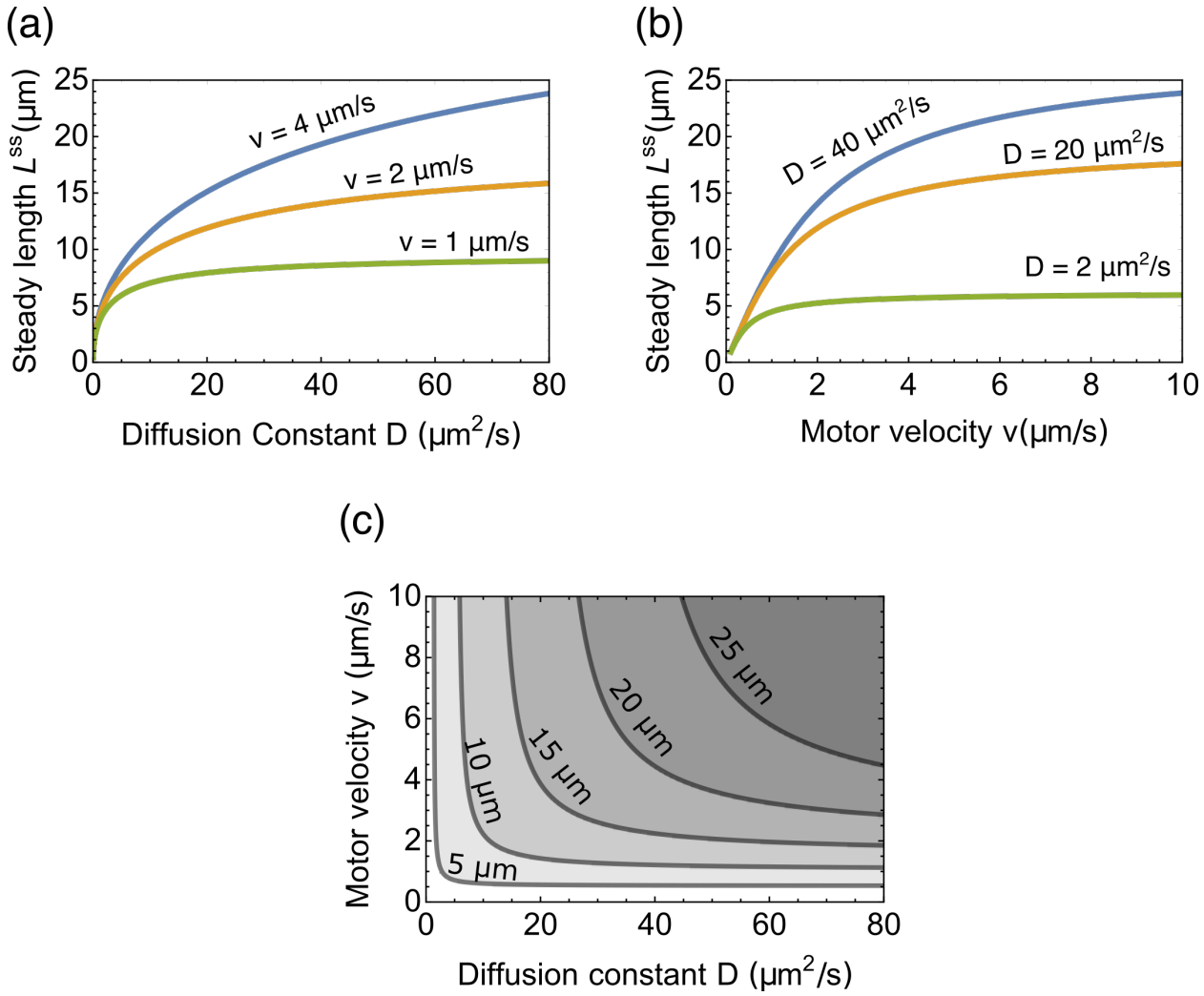

Figure 2.4: Influence of the motor velocity v and diffusion coefficient D on the steady-state length L^{ss} of the flagellum
(a) The steady-state length L^{ss} as a function of diffusion coefficient D for different motor velocities. (b) The steady-state length L^{ss} as a function of motor velocity v for different diffusion coefficients. (c) The contour plot of L^{ss} as a function of both diffusion coefficient D and motor velocity v.

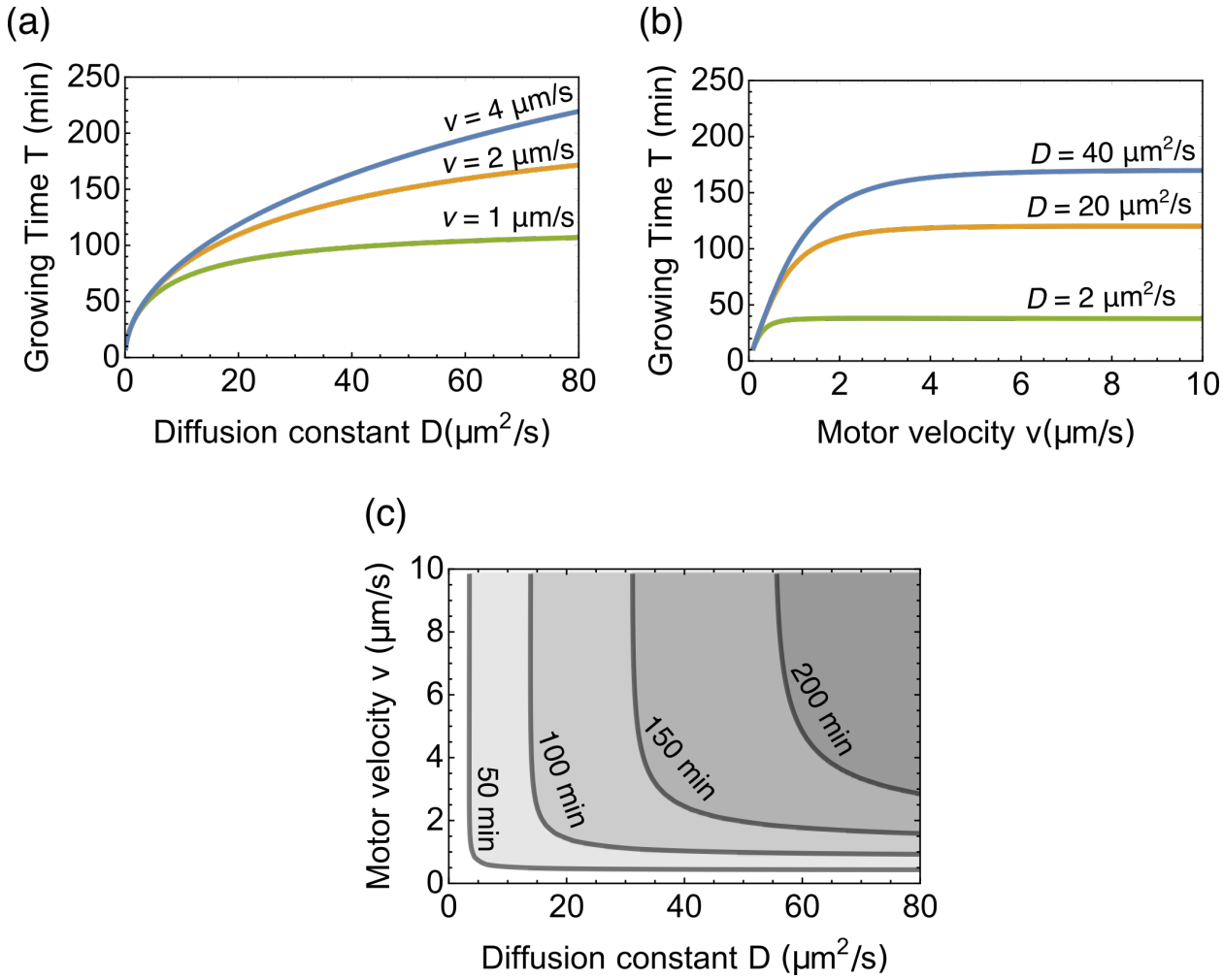

Figure 2.5: Influence of the motor velocity v and diffusion coefficient D on the growing time T of the flagellum
(a) The growing time T as a function of diffusion coefficient D for different motor velocities. (b) The growing time T as a function of motor velocity v for different diffusion coefficients. (c) The contour plot of T as a function of both diffusion coefficient D and motor velocity v.

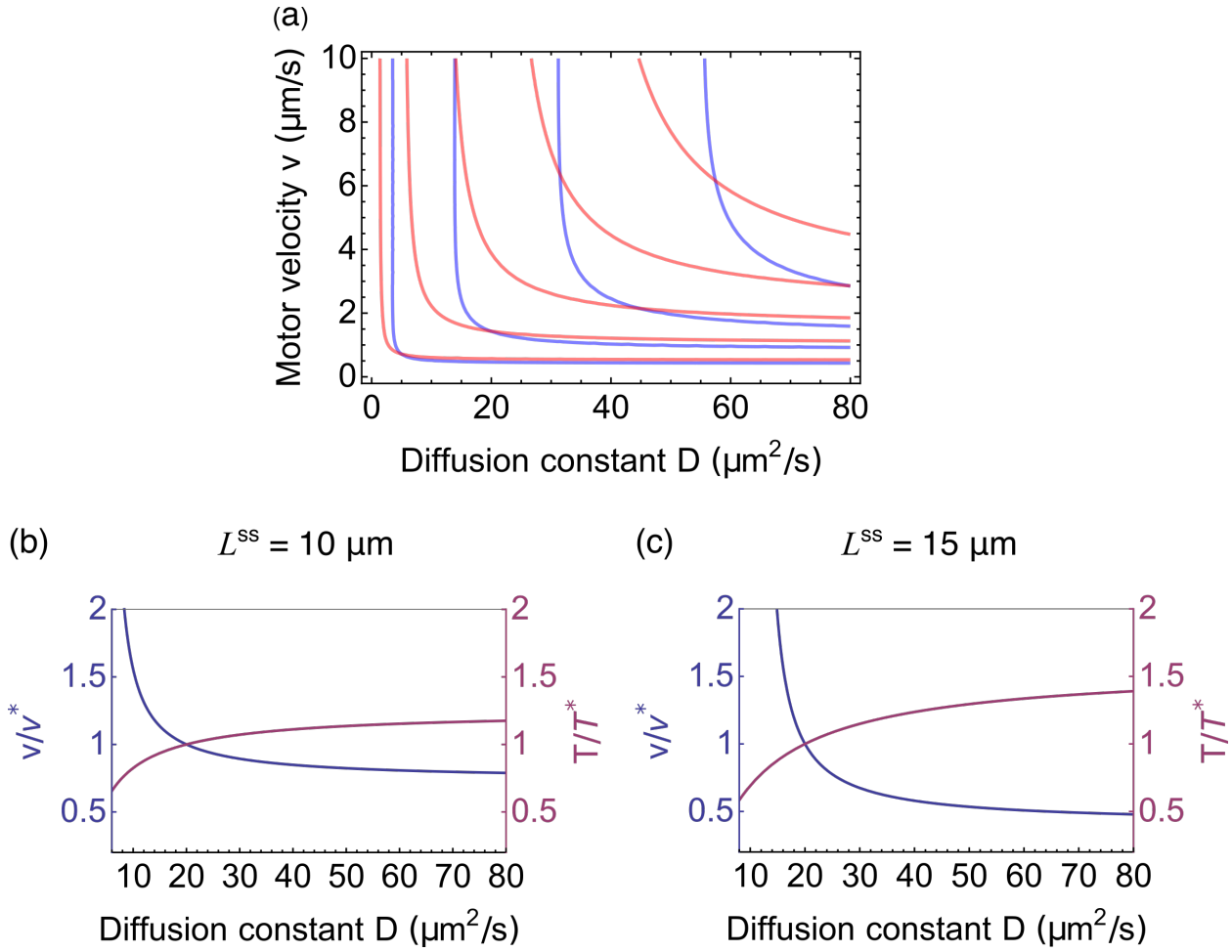

Figure 2.6: Possible parameter changes that keep the steady-state length $\boldsymbol{L^{ss}}$ constant while altering the growing time $\boldsymbol{T}$

(a) Overlay of the contour plots for growing time T (blue) and for steady-state length L^{ss} (red). From left to right, the contours for growing time T are 50, 100, 150, and 200 min, and for steady-state length L^{ss} are 5, 10, 15, 20, and 25 μm. (b, c) Relative change of motor velocity (left axis) and growing time (right axis) as a function of the diffusion coefficient along the contour of $L^{ss} = 10\mu\text{m}$ in (b) and $L^{ss} = 15\mu\text{m}$ in (c). The reference velocity is defined as $v^* = v(D = 20\mu\text{m}^2/\text{s})$ and the reference growing time $T^* = T(D = 20\mu\text{m}^2/\text{s})$.

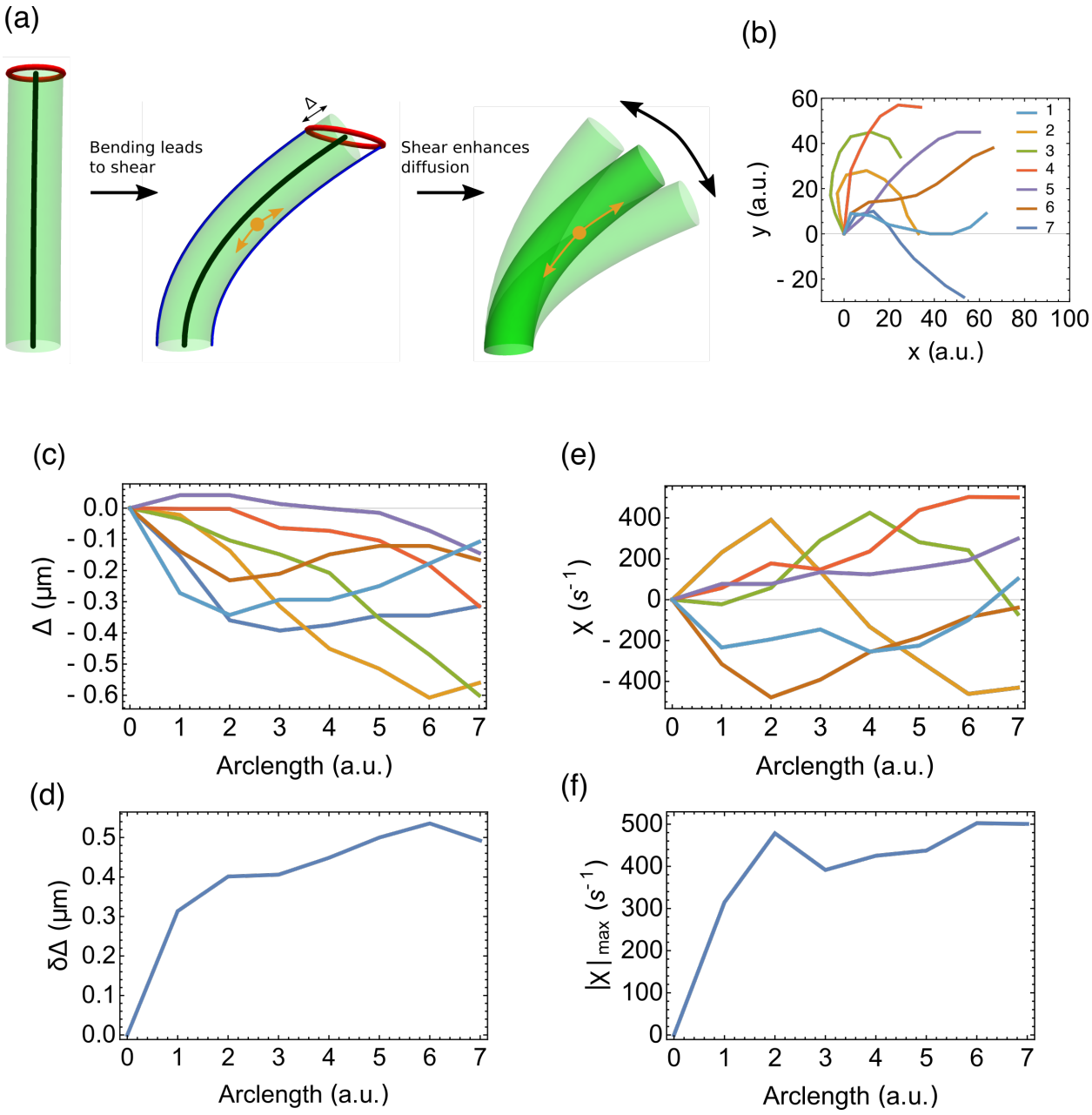

Figure 2.7: Beating of the flagellum leads to enhanced diffusion of motors. (a) The flagellum is depicted as a rod. Bending of the rod leads to stretching on one side and compression on the other side. The two blue curves represent curves on the rod's surface that have the same length as the central axis (black line). The red circle represents all the end points on the rod's surface that have the same length with the central axis. The shear induced by periodic beating of the flagellum can enhance the diffusion of molecular motors via the shear-thinning mechanism, thus increasing the length of flagella compared to paralyzed mutants. (b) Selected beating shapes of a flagellum in a beating cycle. The number indicates the order of the sequence. (c, d) Shear

displacements Δ in (c) and its variation $\delta\Delta$ in a beating period in (d). (e, f) Shear rates χ in (c) and its maximum in a beating period in (f).

Author Contributions:

RM, NLH, WFM, and HQ designed research. RM and NLH performed research and contributed analytic tools. RM, NLH, WFM, and HQ analyzed data. NLH, RM, HQ and WFM wrote the manuscript.

Acknowledgments

This work was initiated, and initial stages of the model developed, at two Cell Modeling Hackathon events supported by NSF grant MCB-1411898. NLH and WFM acknowledge support of NIH grant R35 GM130327.

References

1. Rosenbaum, J.L., J.E. Moulder, and D.L. Ringo. 1969. Flagellar elongation and shortening in Chlamydomonas. The use of cycloheximide and colchicine to study the synthesis and assembly of flagellar proteins. *J. Cell Biol.* 41:600–619.

2. Hendel, N.L., M. Thomson, and W.F. Marshall. 2018. Diffusion as a Ruler: Modeling Kinesin Diffusion as a Length Sensor for Intraflagellar Transport. *Biophys. J.* 114:663–674.

3. Fai, T.G., L. Mohapatra, P. Kar, J. Kondev, and A. Amir. 2019. Length regulation of multiple flagella that self-assemble from a shared pool of components. *eLife*. 8:e42599.

4. Cole, D.G., D.R. Diener, A.L. Himelblau, P.L. Beech, J.C. Fuster, and J.L. Rosenbaum. 1998. Chlamydomonas kinesin-II-dependent intraflagellar transport (IFT): IFT particles contain proteins required for ciliary assembly in Caenorhabditis elegans sensory neurons. *J. Cell Biol.* 141:993–1008.

5. Scholey, J.M. 2003. Intraflagellar transport. *Annu. Rev. Cell Dev. Biol.* 19:423–443.

6. Taschner, M., and E. Lorentzen. 2016. The Intraflagellar Transport Machinery. *Cold Spring Harb. Perspect. Biol.* 8.

7. Lechtreck, K.F., J.C. Van De Weghe, J.A. Harris, and P. Liu. 2017. Protein transport in growing and steady-state cilia. *Traffic Cph. Den.* 18:277–286.

8. Qin, H., D.R. Diener, S. Geimer, D.G. Cole, and J.L. Rosenbaum. 2004. Intraflagellar transport (IFT) cargo: IFT transports flagellar precursors to the tip and turnover products to the cell body. *J. Cell Biol.* 164:255–266.

9. Stepanek, L., and G. Pigino. 2016. Microtubule doublets are double-track railways for intraflagellar transport trains. *Science*. 352:721–724.

10. Vannuccini, E., E. Paccagnini, F. Cantele, M. Gentile, D. Dini, F. Fino, D. Diener, C. Mencarelli, and P. Lupetti. 2016. Two classes of short intraflagellar transport train with different 3D structures are present in Chlamydomonas flagella. *J. Cell Sci.* 129:2064–2074.

11. Kozminski, K.G., P.L. Beech, and J.L. Rosenbaum. 1995. The Chlamydomonas kinesin-like protein FLA10 is involved in motility associated with the flagellar membrane. *J. Cell Biol.* 131:1517–1527.

12. Mueller, J., C.A. Perrone, R. Bower, D.G. Cole, and M.E. Porter. 2005. The FLA3 KAP Subunit Is Required for Localization of Kinesin-2 to the Site of Flagellar Assembly and Processive Anterograde Intraflagellar Transport. *Mol. Biol. Cell*. 16:1341–1354.

13. Marshall, W.F., and J.L. Rosenbaum. 2001. Intraflagellar transport balances continuous turnover of outer doublet microtubules: implications for flagellar length control. *J. Cell Biol.* 155:405–414.

14. Marshall, W.F., H. Qin, M.R. Brenni, and J.L. Rosenbaum. 2005. Flagellar Length Control System: Testing a Simple Model Based on Intraflagellar Transport and Turnover. *Mol. Biol. Cell*. 16:270–278.

15. Porter, M.E., R. Bower, J.A. Knott, P. Byrd, and W. Dentler. 1999. Cytoplasmic dynein heavy chain 1b is required for flagellar assembly in Chlamydomonas. *Mol. Biol. Cell*. 10:693–712.

16. Pazour, G.J., B.L. Dickert, and G.B. Witman. 1999. The DHC1b (DHC2) isoform of cytoplasmic dynein is required for flagellar assembly. *J. Cell Biol.* 144:473–481.

17. Deane, J.A., D.G. Cole, E.S. Seeley, D.R. Diener, and J.L. Rosenbaum. 2001. Localization of intraflagellar transport protein IFT52 identifies basal body transitional fibers as the docking site for IFT particles. *Curr. Biol. CB*. 11:1586–1590.

18. Ludington, W.B., K.A. Wemmer, K.F. Lechtreck, G.B. Witman, and W.F. Marshall. 2013. Avalanche-like behavior in ciliary import. *Proc. Natl. Acad. Sci.* 110:3925–3930.

19. Engel, B.D., W.B. Ludington, and W.F. Marshall. 2009. Intraflagellar transport particle size scales inversely with flagellar length: revisiting the balance-point length control model. *J. Cell Biol.* 187:81–89.

20. Ludington, W.B., H. Ishikawa, Y.V. Serebrenik, A. Ritter, R.A. Hernandez-Lopez, J. Gunzenhauser, E. Kannegaard, and W.F. Marshall. 2015. A Systematic Comparison of Mathematical Models for Inherent Measurement of Ciliary Length: How a Cell Can Measure Length and Volume. *Biophys. J.* 108:1361–1379.

21. Ishikawa, H., and W.F. Marshall. 2017. Testing the time-of-flight model for flagellar length sensing. *Mol. Biol. Cell*. 28:3447–3456.

22. Chien, A., S.M. Shih, R. Bower, D. Tritschler, M.E. Porter, and A. Yildiz. 2017. Dynamics of the IFT machinery at the ciliary tip. *eLife*. 6:e28606.

23. Engel, B.D., H. Ishikawa, K.A. Wemmer, S. Geimer, K. Wakabayashi, M. Hirono, B. Craige, G.J. Pazour, G.B. Witman, R. Kamiya, and W.F. Marshall. 2012. The role of

retrograde intraflagellar transport in flagellar assembly, maintenance, and function. *J. Cell Biol.* 199:151–167.

24. Avasthi, P., M. Onishi, J. Karpiak, R. Yamamoto, L. Mackinder, M.C. Jonikas, W.S. Sale, B. Shoichet, J.R. Pringle, and W.F. Marshall. 2014. Actin Is Required for IFT Regulation in Chlamydomonas reinhardtii. *Curr. Biol.* 24:2025–2032.

25. Lan, Y., and G.A. Papoian. 2008. The Stochastic Dynamics of Filopodial Growth. *Biophys. J.* 94:3839–3852.

26. Naoz, M., U. Manor, H. Sakaguchi, B. Kachar, and N.S. Gov. 2008. Protein localization by actin treadmilling and molecular motors regulates stereocilia shape and treadmilling rate. *Biophys. J.* 95:5706–5718.

27. Zhuravlev, P.I., Y. Lan, M.S. Minakova, and G.A. Papoian. 2012. Theory of active transport in filopodia and stereocilia. *Proc. Natl. Acad. Sci.* 109:10849–10854.

28. Fai, T.G., L. Mohapatra, P. Kar, J. Kondev, and A. Amir. 2019. Length regulation of multiple flagella that self-assemble from a shared pool of components. *eLife*. 8:e42599.

29. Schoppmeier, J., and K.-F. Lechtreck. 2003. Flagellar Regeneration in Spermatozopsis Similis (chlorophyta). *J. Phycol.* 39:918–922.

30. Kannegaard, E., E.H. Rego, S. Schuck, J.L. Feldman, and W.F. Marshall. 2014. Quantitative analysis and modeling of katanin function in flagellar length control. *Mol. Biol. Cell*. 25:3686–3698.

31. Kubo, T., M. Hirono, T. Aikawa, R. Kamiya, and G.B. Witman. 2015. Reduced tubulin polyglutamylation suppresses flagellar shortness in Chlamydomonas. *Mol. Biol. Cell*. 26:2810–2822.

32. Zhu, X., E. Poghosyan, R. Gopal, Y. Liu, K.S. Ciruelas, Y. Maizy, D.R. Diener, S.M. King, T. Ishikawa, and P. Yang. 2017. General and specific promotion of flagellar assembly by a flagellar nucleoside diphosphate kinase. *Mol. Biol. Cell*. 28:3029–3042.

33. Kato, T., O. Kagami, T. Yagi, and R. Kamiya. 1993. Isolation of two species of Chlamydomonas reinhardtii flagellar mutants, ida5 and ida6, that lack a newly identified heavy chain of the inner dynein arm. *Cell Struct. Funct.* 18:371–377.

34. King, S.J., and S.K. Dutcher. 1997. Phosphoregulation of an Inner Dynein Arm Complex in Chlamydomonas reinhardtii Is Altered in Phototactic Mutant Strains. *J. Cell Biol.* 136:177–191.

35. Piperno, G., K. Mead, and W. Shestak. 1992. The inner dynein arms I2 interact with a "dynein regulatory complex" in Chlamydomonas flagella. *J. Cell Biol.* 118:1455–1463.

36. Kamiya, R., and G.B. Witman. 1984. Submicromolar levels of calcium control the balance of beating between the two flagella in demembranated models of Chlamydomonas. *J. Cell Biol.* 98:97–107.

37. Sengupta, S., K.K. Dey, H.S. Muddana, T. Tabouillot, M.E. Ibele, P.J. Butler, and A. Sen. 2013. Enzyme Molecules as Nanomotors. *J. Am. Chem. Soc.* 135:1406–1414.

38. Xu, Z., and A. del Campo. 2019. Probing the Full Distribution of Many-Body Observables By Single-Qubit Interferometry. *Phys. Rev. Lett.* 122:160602.

39. Riedel-Kruse, I.H., A. Hilfinger, J. Howard, and F. Jülicher. 2007. How molecular motors shape the flagellar beat. *HFSP J.* 1:192–208.

40. Yanagisawa, H., G. Mathis, T. Oda, M. Hirono, E.A. Richey, H. Ishikawa, W.F. Marshall, M. Kikkawa, and H. Qin. 2014. FAP20 is an inner junction protein of doublet microtubules essential for both the planar asymmetrical waveform and stability of flagella in Chlamydomonas. *Mol. Biol. Cell*. 25:1472–1483.

41. Taylor, G.I. 1953. Dispersion of soluble matter in solvent flowing slowly through a tube. *Proc. R. Soc. Lond. Ser. Math. Phys. Sci.* 219:186–203.

42. Renaud, M., N. Belgacem, and M. Rinaudo. 2005. Rheological behaviour of polysaccharide aqueous solutions. *Polymer*. 46:12348–12358.

43. Wu, Y., Z.Y. (William) Lin, A.C. Wenger, K.C. Tam, and X. (Shirley) Tang. 2018. 3D bioprinting of liver-mimetic construct with alginate/cellulose nanocrystal hybrid bioink. *Bioprinting*. 9:1–6.

44. Hilton, L.K., K. Gunawardane, J.W. Kim, M.C. Schwarz, and L.M. Quarmby. 2013. The Kinases LF4 and CNK2 Control Ciliary Length by Feedback Regulation of Assembly and Disassembly Rates. *Curr. Biol.* 23:2208–2214.

Publishing Agreement

It is the policy of the University to encourage open access and broad distribution of all theses, dissertations, and manuscripts. The Graduate Division will facilitate the distribution of UCSF theses, dissertations, and manuscripts to the UCSF Library for open access and distribution. UCSF will make such theses, dissertations, and manuscripts accessible to the public and will take reasonable steps to preserve these works in perpetuity.

I hereby grant the non-exclusive, perpetual right to The Regents of the University of California to reproduce, publicly display, distribute, preserve, and publish copies of my thesis, dissertation, or manuscript in any form or media, now existing or later derived, including access online for teaching, research, and public service purposes.

DocuSigned by:
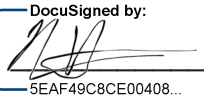
5EAF49C8CE00408...

Author Signature

12/15/2020

Date